CHALMERS
UNIVERSITY OF TECHNOLOGY

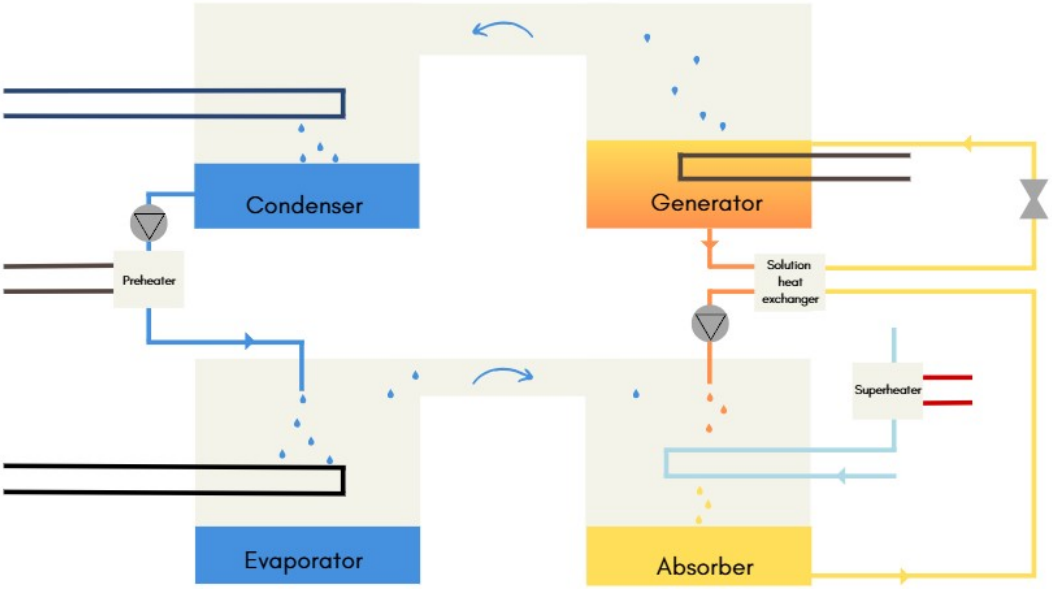

Regeneration of Medium Pressure Steam

A Case Study on Energy Integration and Fresh Water Reduction

Master's Thesis in Sustainable Energy Systems and Innovative and Sustainable Chemical Engineering

ELLA HANSEN
ELLEN JOHANSSON

DEPARTMENT OF CHEMISTRY AND CHEMICAL ENGINEERING
CHALMERS UNIVERSITY OF TECHNOLOGY
Gothenburg, Sweden 2025
www.chalmers.se

Master's thesis 2025

Regeneration of Medium Pressure Steam

A Case Study on Energy Integration and Fresh Water Reduction

ELLA HANSEN
ELLEN JOHANSSON

CHALMERS
UNIVERSITY OF TECHNOLOGY

Department of Chemistry and Chemical Engineering
Division of Chemical Reaction Engineering
Chalmers University of Technology
Gothenburg, Sweden 2025

Regeneration of Medium Pressure Steam
A Case Study on Energy Integration and Fresh Water Reduction
ELLA HANSEN
ELLEN JOHANSSON

Supervisor: David Norsund, Borealis
Examiner: Prof. Derek Claude Creaser, Department of Chemistry and Chemical Engineering

Master's Thesis 2025
Department of Chemistry sand Chemical Engineering
Division of Chemical Reaction Engineering
Chalmers University of Technology
SE-412 96 Gothenburg
Telephone +46 31 772 1000

Cover: Visualization of Absorption Heat Pump.

Typeset in LaTeX
Printed by Chalmers Reproservice
Gothenburg, Sweden 2025

1

Abstract

Borealis is a world leading producer of polyolefins [1]. In Stenungsund, Borealis is divided into two separate sites where the cracker produces ethylene gas, and the polyethylene plant produces polyethylene mainly for power cables. This work focuses on the cracker plant, and investigates the possibilities of reducing fresh water intake by utilizing waste heat to produce steam needed for cracking. The objectives of this thesis are to investigate how much medium pressure steam used for cracking, so called dilution steam (DS), can be recovered, how much fresh water can be saved, how this integration would affect the overall steam system, how much fuel gas this integration could save, and if the CO_2-emissions could be reduced. Furthermore, it also served to investigate whether the water being recycled needs to be purified and how much the investment as a whole would cost the company.

The method used for answering these questions was a mixture of a literature study and simulations in Aspen Hysys ®, Aspen Plus ® and Aspen EDR ®, as well as calculations in Microsoft Excel. The literature studies was the first step in the workflow, where information about industrial solutions that utilizes waste heat and lifts it to higher temperatures were searched for. One of the greatest challenges with this work was to find a configuration that could lift waste heat from 112 °C to a temperature high enough to produce Dilution Steam (DS) of 240 °C. Several solutions such as Closed Cycle Compressor (CCC), Mechanical Vapor Re-compression (MVR) and Absorption Heat Pumps (AHP) were found in literature, and were simulated in Aspen Hysys ® and Aspen Plus in various configurations. Unfortunately, all where too energy demanding to be economically viable. However, eventually the Absorption Heat Transformer (AHT) was found and simulated. This solution, when run at the right temperatures and pressures, could heat the recycled water, which was the water exiting the cracker site's sour water stripper system unit, to 182 °C while also evaporating it entirely. For the final configuration, another waste heat source from the quench heat exchangers was also utilized. In order to heat the 182 °C stripper water to 240 °C, high pressure (HP) steam was used after the AHT. A DS flow of 16.4 ton/h was obtained. It was also specified that DS should hold a pressure of 9.8 bar, which was solved by pressurizing the stripper water with a pump before entering the AHT.

The AHT design resulted in a Coefficient of Performance (COP) of 0.29, an investment cost of between 175 and 317 MSEK, and a pay back period (PBP) of between three and six years based on current prices. The PBP however varied between 1.7 and 27.8 years depending how prices of electricity, fuel gas, CO_2-emission rights and fresh water could vary in the future. In other words, one of the conclusions that could be drawn was that the AHT investment was quite sensitive to price changes. The cost was computed through two different paths: via Nusselt's correlations and cost equations computed in Excel, and via Aspen EDR.

It was further concluded that an implementation of the AHT would decrease the fuel gas use, CO_2-emissions, fresh water intake, while simultaneously utilize waste heat and generate DS from recirculated water.

Acknowledgements

First and foremost, we would like to thank Borealis for the opportunity to learn more about their process at the cracker site. With a welcoming attitude and an always helping hand, we have been guided trough our work. Thanks to the colleagues at the Asset Development department at Borealis cracker for their help and support. A special thank you to our supervisor David Norsund, process engineer at Borealis, who always set aside time for us when we were faced with a problem. He has been very inspiring and no questions were too dumb to ask.

Furthermore we would like to thank our examiner Derek Claude Creaser, full professor in chemical engineering, for his fast feedback and availability. With his carefree attitude he always made time for our questions and problems.

Last but not least we would like to thank Judit Fortet Casabella for her interest in our project despite not being a supervisor. She has given us very valuable feedback and inspired us with her knowledge in the area of energy applications.

Ella Hansen, Ellen Johansson, Gothenburg, May 2025

2

Nomenclature

2.0.1 Abbreviations

AHP	Absorption Heat Pump
AHT	Absorption Heat Transformer
ANP	Anual Net Profit
BET	Biological Cleaning Facility
CCC	Closed Cycle Compression
CF	Cash Flow
COP	Coefficient of Performance
DS	Dilution Steam
EDR	Exchanger Design and Rating
EGT	Electricity Generating Turbine
ETS	Emission Trading System
EU	European Union
GHG	Green House Gases
HDPE	High Density Polyethylene
HP	High Pressure
ISBL	Inside Battery Limits
LDPE	Low Density Ethylene
LiBr	Lithium Bromide
LP	Low Pressure
MVR	Mechanical Vapor Re-compression
NPV	Net Present Value
PBP	Pay Back Period
TEMA	Tubular Exchanger Manufacturers Association

2.0.2 Symbols

A	Area	[m^2]
a_L	Thermal diffusivity	$[\frac{m^2}{s}]$
Bo	Boiling number	-
C_e	Equipment cost	[SEK]
C_p	Heat capacity	$[\frac{J}{kg°C}]$
c_m	Cost per mass	$[\frac{SEK}{kg}]$
CF_n	Cash flow	-
COP	Coefficient of performance	
d	Diameter	[m]
D_b	Tube bundle diameter	[m]
€	Euro	[Euro]
f_f	Friction Factor	-
F_t	F-factor	-
Fr	Froude number	-
G	Mass flow rate per cross sectional area	$[\frac{kg}{m^2s}]$
g	Gravitational force	$[\frac{m}{s^2}]$
h	Heat transfer coefficient	$[\frac{W}{m^2°C}]$
h	Enthalpy	$[\frac{kJ}{kg}]$
HV_{eff}	Effective heating value	$[\frac{kJ}{kg}]$
h_{fg}	Heat of vaporization	$[\frac{J}{kg}]$
i	Interest rate	-
j_f	Friction factor	-
j_h	jh-factor	-
k	Conductivity	$[\frac{W}{m^2°C}]$
l	Length	[m]
M	Molar mass	$[\frac{g}{mol}]$
$\dot{m}$	Mass flow	$[\frac{kg}{s}]$
n	Year	[Year]
N_t	Number of tubes	-
Nu	Nusselts number	-
P	Effect	[W]
p_t	Tube pitch	[m]

Pr	Prandtls number	-
Q	Energy	[J]
R	Revenue	$[\frac{SEK}{kg}]$
R	Gas constant	$[\frac{J}{molK}]$
Re	Reynolds number	-
S	Area	[m^2]
St	Stantons number	-
T	Temperature	[°C]
t	Operating hour	$[\frac{hours}{year}]$
U	Overall transferrer coefficient	$[\frac{W}{m^{2\circ}C}]$
W	Effect	[J/s]
W_c	Total condensate flow	$[\frac{kg}{s}]$
q	Heat flux	$[\frac{W}{m^2}]$
x	Vapor fraction	-
ΔP	Pressure drop	[Pa]
ΔT	Temperature difference	[°C]
ΔT_{LM}	Logarithmic mean temperature difference	[°C]
Γ	Vertical tube loading	$[\frac{kg}{ms}]$
Σ	Sum	-
Σh_L	Head loss	[Pa]
$^\circ C$	Degree Celsius	[$^\circ C$]
γ	Correction factor	-
μ	Viscosity	[Pas]
ν_∞	Velocity	-
π	Pi = 3.14	-
ψ	Two phase multiplier	-
ρ	Density	$[\frac{kg}{m^3}]$
σ	Surface tension	$[\frac{N}{m}]$

2.0.3 Indices

B	Baffle
c	Condensation
D	Diameter
e	Hydraulic*
el	Electricity
HP	High pressure steam
i	Inner
id	Inner diameter
L	Liquid
LM	Logaritmic mean
m	Mean
n	Year
o	Outer
od	Outer diameter
p	Pressure
$sat.liq$	Saturated liquid
$sat.vap$	Saturated vapor
sh	Super heated
T	Temperature
t	Tube
th	Thermal
tp	Two phase
v	Vapor
w	wall

* The ratio of the wet cross-sectional area to the wet perimeter of a water-carrying pipe.

Contents

List of Figures

List of Tables

3
Introduction

Water scarcity is becoming an increasing problem around the world. Water extraction in Europe has decreased with 19% since 2000, yet the area and people affected by water scarcity have increased [2]. Water scarcity is also believed to increase as a consequence of climate change. Sweden has historically been one of the countries least affected by water scarcity in the European Union, but it is still important to be mindful of resource use. The industries in Sweden use 70% of the water extracted compared to the rest of EU where this figure is 40%.[3]. Industries play an important part to enable a secure water access in the future when droughts will become more frequent. The paper and pulp industries are the largest consumers of water in Sweden, followed by chemical and pharmaceutical industries.

Borealis in Stenungsund produces high density polyethylene (HDPE) and low density polyethylene (LDPE) from naphtha, propane, ethane and liquefied petroleum gas (LPG). The feedstock is cracked in furnaces which generates ethylene. The ethylene is then polymerized to HDPE and LDPE at the neighboring polyethylene plant. The cracking process consumes a large amount of water since steam is needed in the furnaces to generate the right operating conditions. This steam is commonly called dilution steam (DS). The DS demand is about 90 tonnes per hour. Heavy hydrocarbons are first separated after the furnaces in the primary fractionation distillation tower, see figure 3.1 below. Quench oil is circulated in the primary fractionating tower to secure a constant liquid flow and ensure a correct operating temperature. This quench oil is cooled down by preheating water which will be turned into steam in the furnaces. The top fraction from the primary fractionation is cooled down in several heat exchangers, called the over head. The chilled process stream is let into the separation tank where three phases are formed: water (blue in figure), liquid hydrocarbons (brown in figure) and hydrocarbons in gas phase (gray in figure). The water phase is parted from the separation tank. This water contains water-soluble hydrocarbons such as phenols which are separated in another distillation tower called the sour water *stripper* tower. The stripped water is further cleaned in a biological cleaning facility, the *BET* and then discharged to the ocean.

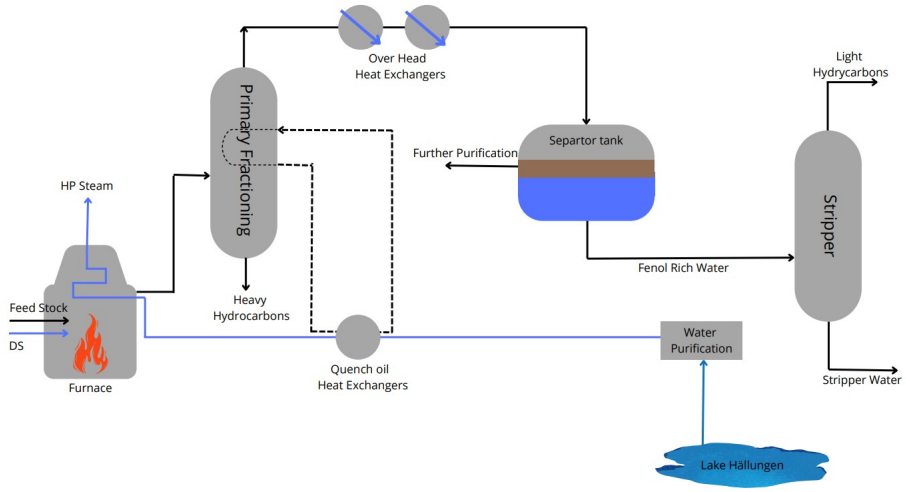

Figure 3.1: Simplified overview of the process at the Borealis Cracker.

HP steam is produced when cooling the process stream and flue gases from the furnaces. The fresh water for steam production is taken from lake Hällungen, and is thereafter purified since high pressure and temperature generate corrosive conditions. Additional steam is also produced from three boilers. Both the furnaces and boilers are powered with fuel gas which is a side product from the cracking process. The fuel gas contains methane and hydrogen that is combusted to generate energy according to reactions shown in equations 3.1 and 3.2 [4].

$$CH_4 + 2O_2 \rightarrow CO_2 + 2H_2O \tag{3.1}$$

$$2H_2 + O_2 \rightarrow 2H_2O \tag{3.2}$$

Since the stripper water is not reused, it generates a high consumption of fresh water at the plant. If this waste water stream can be recirculated and used for DS, the water demand of the factory could be reduced. This would be a positive adaption for the Borealis cracker, as the current water purification facility is near its limit of being overloaded and the plant is also at its limit of allowed water extraction from the freshwater lake. Generation of DS by waste heat would also decrease the amount of HP steam needed and thereby potentially reduce the amount of fuel gas combusted.

There are three pressure levels in the steam system at the Borealis cracker: high pressure (HP) of 86 bar, medium pressure (MP) of 9.8 bar, and low pressure (LP) of 1.9 bar. The furnaces produce HP steam as a consequence of the cracking process due to the excess heat, and additional boilers produce HP to balance the system. A lot of the HP steam is used for generating electricity in an electricity generating turbine (EGT), while some is used in reactors at the polyethylene plant. At the end, it is recycled back to feed water, despite some steam that is used for steam tracing, dilution steam for the furnaces, and steam for the flare.

3.1 Objectives and Purpose

The main objective of this thesis is to investigate whether it is possible to recirculate waste water to produce dilution steam to the steam cracking furnaces. This question is of great interest in order to reduce the factory fresh water use. First it is necessary to establish the purity needed as it will effect the design and integration of such a system. Moreover it will also be investigated how such an integration will affect the steam system at the plant.

The objective is formatted into the following six questions:

- How much dilution steam can be recovered and how much fresh water does this save?
- How is the steam system affected by recovering dilution steam?
- How much fuel gas can be saved?
- Does the waste water need to be purified to enable its reuse for dilution steam?
- How much could a dilution steam recovery integration potentially decrease CO_2 emissions?
- Is it possible to design an integration that is economically favorable for the process?

The main question to be answered is how much dilution steam can be recovered by heating water with excess heat instead of fuel gas. This may generate excess fuel gas. If so, it will be of interest to examine how much excess is generated and what applications or usage it might have.

3.2 Limitations

In this section, limitations regarding the project are described. More specific and detailed limitations regarding calculations and simulations are described in the Method in the workflow.

One limitation made in this work was disregarding how the performance of the separation tank was affected by the utilization of the overhead in the AHT. It was also disregarded how the DS entered the furnaces and what happened inside the furnaces. Moreover, it was not looked into how the fuel gas excess would affect the equipment and system. Also, the operational consequences of taking a boiler out of operation were overlooked.

Regarding the water purity needed for DS generation, no specific solution was calculated or simulated for the purification.

4

Theory

4.0.1 Heat Pumps

Heat pumps can be used to upgrade waste heat or low grade heat to enable applications at higher temperatures [5]. To do so, additional work input is often required, either by a pump or compressor. Common heat pumps are Mechanical Vapor Re-compressors (MVR), Closed Cycle Compressors (CCC) and Absorption Heat Pumps (AHP).

High-temperature industrial heat pumps have not been well established on the market until recently [6]. Commonly they are used for producing lower grade heat, for example district heating, of at most around 80°C [7]. However, it is predicted that the use of industrial heat pumps will increase by 15% per year until 2030 [6]. They are also predicted to make up a larger part of the energy generation in industries, with an increase by 22% until 2030.

For a heat pump the Coefficient of Performance, COP is defined as in equations 4.1.

$$COP = \frac{Heating\ Power}{Compressor\ Power\ Consumption} = \frac{T_1}{T_1 - T_2} \tag{4.1}$$

The Carnot Efficiency can then be computed, which is a ratio of how close the heat pump is to the theoretically maximum of a refrigeration heat pump. The Carnot Efficiency can be viewed in equation 4.2.

$$\eta_{carnot} = \frac{COP}{COP_{carnot}} = \frac{T_1 - T_2}{T_1} \tag{4.2}$$

The thermal efficiency for a heat engine is as follows in equation 4.3.

$$\eta_{th} = \frac{Power\ Consumptiont}{Heating\ Power} = \frac{W}{Q_1} < \eta_c \tag{4.3}$$

4.0.1.1 CCC

A CCC heat pump is a closed cycle where a refrigerant is circulated. The cycle consists of an evaporator, a compressor, a condenser and a throttle valve [8]. The cycle is configured in a way where the refrigerant is evaporated, then compressed, whereupon it is condensed and then throttled back to the evaporator pressure again to start over. This means that work is put into the compressor and heat is released at a higher temperature in the condenser due to the increase in temperature and pressure. This concept allows for low value streams of lower temperatures, to generate heat when electricity is added, which entails a temperature lift.

The purpose of the compressor is to generate a higher pressure of the evaporated fluid, which will result in an increase in temperature, according to equation 4.4 [9].

$$\frac{T_2}{T_1} = (\frac{P_2}{P_1})^{R/C_p} \tag{4.4}$$

Further, the condenser is a heat exchanger that uses a cold stream to cool the hot gas generated in the compressor to the saturation point, and then condenses it [8]. It is the temperature difference between the process stream entering the evaporator, and the process stream exiting the condenser that gives the temperature lift of the heat pump. The condenser pressure is higher than the evaporator pressure, hence the refrigerant needs to go through an expansion valve in order to decrease in temperature before entering the evaporator again.

The choice of refrigerant is of great importance, as it affects the efficiency of the heat pump. There are several factors to consider when selecting refrigerant, such as toxicity, global warming potential, vapor pressure, heat transfer ability and COP [8]. It is also important that the boiling point of the refrigerant lays in between the interval in which the heat source is cooled in the evaporator. Ideally, a refrigerant should be chosen so that it is superheated in the evaporator. In figure A.1 in Appendix, section A, suitable working fluids for different temperature and pressure conditions can be viewed.

4.0.1.2 MVR

An MVR is an open heat pump. This means that, in comparison to a closed cycle heat pump, no refrigerant is used, and the fluid is evaporated and compressed directly to inflict a temperature lift. The concept of an MVR pump is to utilize a low value stream, either in liquid or vapor state, and produce a higher value vapor stream by adding electricity work directly to the stream considered. This mechanism begins with leading the process liquid into an evaporator to vaporize it, and thereafter compress the vapor to a higher temperature and pressure. The next step is generally to condense the compressed vapor, and this is where heat can be released.

There are several configuration alternatives for the MVR. For example, a two-stage compressor can be used with intermediate cooling to reach even higher pressures. Also, the process liquid can be pressurized before entering the evaporator to decrease the compressor work. The compressor and evaporator work the same in the MVR as in the CCC, despite the fact that the process liquid is handled instead of a refrigerant.

4.0.1.3 AHP and AHT

There are two types of absorption heat pumps, type-I and type-II [10]. Type I, normally called Absorption Heat Pump (AHP) amplifies low grade heat with high temperature heat to generate more amount of heat at medium temperature than what was inputted as low grade heat, see schematic figure below. Type II, also called Absorption Heat Transformer (AHT), uses a medium temperature heat source and upgrades it to a high temperature heat and a low grade heat.

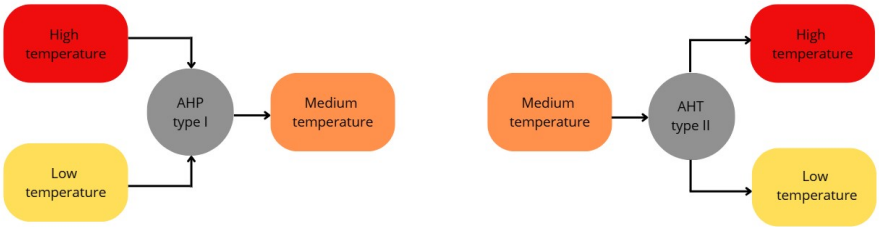

Figure 4.1: Schematic representation of an AHP (left) and an AHT (right).

An AHP consists of an evaporator, condenser, generator and absorber [10]. The evaporator and absorber operate at low pressure while the condenser and generator operate at high pressure. Low-grade heat is used to evaporate the working fluid. The working fluid consists of a working pair. Lithium-bromide (LiBr) and water, or ammonia and water are commonly used. LiBr has a boiling

point of 1265 °C while ammonia has a boiling point of -33 °C [11] [12]. However, they work opposite to each other. In the LiBr-water working pair, it is the water that absorbs in the LiBr-solution, and in the ammonia-water working pair it is the ammonia that is evaporated and then absorbed in the water. When deciding which working pair should be chosen, it is hence the boiling point of water that should be compared with the one of LiBr when finding a match for the process in mind. The LiBr-water solution has been proven to perform better than the ammonia-water working fluid pair in AHPs regarding efficiency [13]. However, using the LiBr-water working pair can entail corrosion, limited solubility, an upper temperature limit, and the solution has a higher viscosity, which can cause problems.

The low pressure enables the working medium to evaporate at lower temperature, by reducing the boiling point. The vapor is then absorbed by the liquid in the absorber [10]. Since the vapor transitions from a vapor stage to a liquid one during the absorption, heat is released. The weak solution is pumped to the generator, where high-grade heat partly evaporates the working medium. The working medium condenses in the condenser while heating the process fluid. The boiling point temperature is increased in the condenser due to the high pressure. This enables the condensation to occur at a higher temperature than the evaporation in the evaporator, thereby resulting in the temperature lift. The liquid in the condenser is let down to the evaporator by a throttle valve to reduce the pressure. Both the heat input in the evaporator and generator are used to generate the amplified heat output in the condenser as well as the additional heat generated by the exothermic reaction in the absorber. Because of this the COP is always larger than one. Due to the vapor being absorbed back into a liquid solution in an AHP, a higher pressure can be achieved with a pump instead of a compressor as in a CCC and MVR, which thereby drastically decreases the electricity demand [14]. For an AHT the electricity demand is only about 1% of the energy output.

An AHT consists of the same equipment as an AHP: a generator, condenser, evaporator, and absorber [10]. The difference between the two types is that in an AHT, medium grade heat is used both in the generator and in the evaporator instead of high grade heat in the generator and low grade heat in the evaporator as in an AHP. Instead of the heat output being in the condenser, the condenser usually releases heat to the surroundings at ambient temperature and the heat output is at the absorber. Since AHT uses one heat source and generates one upgraded heat source and waste heat at ambient temperature, COP will always be less than one, commonly around 0.3. The working principles of the evaporator, absorber, generator, and condenser are the same in both types, but in an AHT the generator and condenser operate at lower pressures than the evaporator and absorber. Due to this, the low grade heat is able to be rejected at ambient temperatures.

Two AHT cycles can be combined to create a double stage and generate a higher temperature lift [10]. The heat output in the absorber is then used as the heat input in the next stage evaporator. In this project, it is assumed that the conditions in the evaporator and generator are saturated. Hence the operating pressure and temperature in an AHT can be determined from steam tables and working fluid diagrams [15].

LiBr exhibits some flaws as a working medium, such as low working pressure, high corrosion rates at high temperatures and risk of crystallization at high concentrations [16]. In the 70s, Carrol ^{TM} was developed by Carrier Corporation, a solution with 1 to 4.5 LiBr to ethylene glycol with respect to weight. The addition of ethylene glycol to the working pair water-LiBr improves thermal physical properties such as viscosity, thermal conductivity as well as maximum concentration before LiBr starts to crystallize. Due to this, the performance of the AHP or AHT is improved. However there is no data available on how the corrosion is affected by the addition of ethylene glycol. To reduce corrosion, lithium molybdate (Li_2MoO_4) can be used. The concentration of lithium molybdate should be kept above 100 ppm [17]. It has been shown to operate as an effective corrosion inhibitor even at temperatures as high as 200°C. A passive film of Fe_2O_3 is formed on steel, halide ions such as Br^- however tend to destroy this film [16] [17]. Li_2MoO_4 forms a second passive oxidized film of MoO_2 on metal surfaces to prevent corrosion.

4.0.1.4 AHT Equipment

An AHT or AHP consist of several heat exchangers. The evaporator, absorber, solution heat exchanger, generator and condenser are all different types of shell and tube heat exchangers. Beside the heat exchangers, a pump to increase the pressure after the condenser and a valve upstream of the generator are needed.

The absorber is a shell and tube heat exchanger with vertically standing tubes within the shell [18]. The cold process liquid goes on the tube side. The evaporator and the generator are connected so that the water vapor flows to the absorber. The concentrated LiBr is sprayed onto the tubes, creating a thin falling film on the tubes. The vapor absorbs into the thin film and the generated absorption heat heats and/or evaporates the cold process fluid.

The solution heat exchanger after the absorber transfers heat from the weak LiBr solution to the concentrated LiBr solution from the generator. The generator is just like the absorber, a shell and tube heat exchanger with vertical tubes. The weak LiBr solution is sprayed onto the tubes, creating a falling film. Within the tubes is a hot process fluid that transfers heat to the LiBr solution and evaporates the water that exits the top of the heat exchanger. The now concentrated LiBr solution is pumped back to the solution heat exchanger.

The reactions considered in the absorber can be viewed in reactions 4.5 to 4.8.

$$LiOH \longleftrightarrow Li^+ + OH^- \tag{4.5}$$

$$HBr + H_2O \longleftrightarrow Br^- + H_3O^+ \tag{4.6}$$

$$2H_2O \longleftrightarrow H_3O^+ + OH^- \tag{4.7}$$

$$LiBr \longrightarrow Li^+ + Br^- \tag{4.8}$$

Reactions 4.5 and 4.6 are the dissolution of water-solved Li^+ and Br^-. Reaction 4.7 is the autoprotolysis of water that is occurring as a side reaction. Reaction 4.8 is the dissociation of LiBr. The main reaction in the absorber can be viewed in 4.9.

$$Li^+ + Br^- + H_2O \longrightarrow LiOH + HBr \ \Delta H = -71.36\frac{kJ}{mol} \tag{4.9}$$

4.0.1.5 AHT Simulation

The generator and absorber, which have a more complex configuration of shell and tube heat exchangers than the other heat exchangers, are more difficult to correctly simulate in Aspen Plus with respect to reality. An equilibrium reactor followed by a cooler could represent the absorber in a quite fair way, as the absorption of water in the LiBr-solution can be viewed as a reaction. This reaction, seen in reactions 4.5 to 4.9, is exothermic and hence releases heat. It is however the condensation mechanism that is the most important factor of heat release. This is what the equilibrium reactor is meant to represent: a temperature increase caused by absorbing the water in the LiBr-solution. The following cooler, cooling the exiting weak LiBr-solution flow, represents the heating of the process fluid on the tube side by heat transfer from the LiBr-solution. In real life, these two steps occur simultaneously, but to simulate it as two steps was considered to be the best alternative in Aspen Plus. Even though the reaction is not of equilibrium characteristics, using the equilibrium reactor appeared to be the best approach considering the alternatives of reactor models in Aspen Plus, seen in table 4.1.

Table 4.1: Different reactor types available in Aspen Plus.

Reactor Type	**Assumptions**
Stoichiometric Reactor	Stoichiometric reactor based on known fractional conversions or extents of reaction.
Yield Reactor	Non stoichiometric reactor based on known yield distribution.
Equilibrium Reactor	Rigorous equilibrium reactor based on stoichiometric approach.
Gibbs Reactor	Rigorous reactor and multiphase equilibrium based on Gibbs free energy minimization.
CSTR	Rigorous stirred tank flow reactor with rate controlled reactions based on known kinetics.
Plug Reactor	Rigorous plug flow reactor with rate controlled reactions based on known kinetics.
Batch Reactor	Rigorous batch or semi batch reactor with rate controlled reactions based on known kinetics.
Electrolyzer	Shortcut and rigorous electrolyzer.

The batch-, plug- and CSTR reactor are all reactors based on known kinetics. These rectors cannot be applied on this work as the kinetics are not of interest in this case, only the amount of heat released. Since we do not have an electrolyzer, this model can be disregarded as well. The Gibbs reactor minimizes the Gibbs free energy in the system and is commonly used for many and complex reactions. The other reactors left are the yield reactor, stoichiometric reactor and equilibrium reactor which all could be used for an approximation of the absorber.

4.0.2 Heat Exchangers

Heat exchangers transfer heat from one medium to another, and is a vital part of most chemical processes [19]. Generally, the media are separated from each other by a wall to allow for heat transfer but avoid mixing or contamination between the two streams. Common types of heat exchangers are plate heat exchangers and shell and tube heat exchangers. Provided that there are no losses, the heat transferred between the fluids can be seen in equation 4.10.

$$Q = Cp \cdot (T_{initial} - T_{final}) \tag{4.10}$$

The area required for heat exchange is dependent on the temperature difference between the fluids and the heat transfer coefficient, U [19]. The temperature difference is calculated differently depending on whether the flows are parallel or countercurrent. For parallel flow the temperature difference, ΔT is simply the mean of the inlet and outlet temperature difference between the fluids. This can be viewed in equation 4.11.

$$\Delta T = \frac{(T_{hot,in} - T_{cold,in}) + (T_{hot,out} - T_{cold,in})}{2} \tag{4.11}$$

For a counter current flow the temperature difference will vary throughout the heat exchanger and is calculated by the logarithmic mean temperature difference, ΔT_{LM}, which can be seen in relation

4.12 [19].

$$\Delta T_{LM} = \frac{\Delta T_1 - \Delta T_2}{ln\frac{\Delta T_1}{\Delta T_2}} \tag{4.12}$$

Where ΔT_1 is the temperature difference between the inlet temperature of the hot stream and the outlet temperature of the cold stream. ΔT_2 is the temperature difference between the outlet temperature of the hot stream and the inlet temperature of the cold stream.

The minimum temperature difference in industrial heat exchangers is commonly 10°C to ensure efficient heat recovery and avoid temperature crosses [8].

Subsequently, the heat transferred between the fluids is visualized in 4.13 [19].

$$Q = A \cdot U \cdot \Delta T \tag{4.13}$$

4.0.2.1 Shell and Tube Heat Exchangers

Shell and tube heat exchangers are widely used within the petrochemical industry due to their robust design and easy maintenance [19]. A shell and tube heat exchanger consist of bundles of tubes in which one media flows. The other fluid surrounds the tubes and is contained within a shell.

The heat transfer area of a shell and tube heat exchangers is dependent of the number of tubes, their length and circumference [19]. This can be seen in equation 4.14.

$$A = N_t \cdot d \cdot \pi \cdot l \tag{4.14}$$

Where N_t is the number of tubes, l is the length and d is the diameter.

Inside a shell and tube heat exchanger are baffles that direct the flow on the shell side and support the tubes [19]. The flow in shell and tube heat exchanger is thereby not truly counter current but a mixture of countercurrent, cross-flow and co-current. To account for this deviation, an F-factor is used. The F-factor is a function of the fluid temperatures, the number of tubes and the number of tube and shell passes. The corrected temperature difference ΔT_m can thereby be seen in equation 4.15.

$$\Delta T_m = F_t \cdot \Delta T_{LM} \tag{4.15}$$

4.0.2.2 Sizing of Shell and Tube Heat Exchangers

In order to calculate the cost of the equipment designed, the sizes of the equipment needs to be known. The sizes of shell and tube heat exchangers can be computed in a multitude of ways depending on factors such as the phase of the working fluids, if a phase change occurs, and whether the fluid is fouling, corrosive, or neither. However, the area is always computed from equation 4.13. The overall heat transfer coefficient U, is always computed as in equation 4.16.

$$\frac{1}{U_o} = \frac{1}{h_o} + \frac{1}{h_{od}} + \frac{d_o ln(\frac{d_o}{d_i})}{2k_w} + \frac{d_o}{d_i} \cdot \frac{1}{h_{id}} + \frac{d_o}{d_i} \cdot \frac{1}{h_i} \tag{4.16}$$

where U_o is the overall heat transfer coefficient based on the tube outside area in W/(m ^{2} °C), h_o is the outside fluid film heat transfer coefficient in W/(m ^{2} °C), h_i is the inside fluid film coefficient in W/(m ^{2} °C), h_{od} is the outside fouling factor in W/(m^2°C), h_{id} is the inside fouling factor in W/(m^2°C), k_w is the thermal conductivity of the tube wall in W/(m°C), and d_o and d_i are the outside and inside tube diameters in m [8].

In shell and tube heat exchangers, heat transfer consists of conduction and convection. The third heat transfer mechanism, radiative heat transfer, is neglected as this phenomena occurs when there

is no transfer medium present [20]. Conduction is characterized of molecular interactions, where molecules at higher energy levels imparts energy to adjacent molecules at lower energy levels [20]. Another conduction mechanism is conduction caused by free electrons on a solid material. Pure metallic solid surfaces have the highest amount of free electrons, which makes them the best conductors. In the case of shell and tube heat exchangers, conduction takes place as heat is transferred through the tube wall and through the process fluids.

Convection occurs between a fluid and an adjacent surface, for example between the tube wall and process fluid [20]. There are two types of convection: forced convection and free convection. Forced convection occurs when an external agent forces the fluid to flow across a surface. The external agent can for example be a pump or fan, and hence it is forced convection that takes place in a shell and tube heat exchanger. Free convection occurs when temperature differences in the fluid causes density differences across the solid surface.

Equation 4.16 takes both convection and conduction into account, where k_w is the conductivity of the tube wall and h_o, h_{od}, h_i and h_{id} are the convective heat transfer coefficients in the fluid inside and outside the tubes. Therefore both convection and conduction are considered.

The calculation of the convective heat transfer coefficient on the tube side, h_i, is computed via Nusselts number. For forced convection for internal turbulent flows, Nusselts number is computed as in equation 4.17. The flow is assumed to be turbulent if it has a value of Reynolds number above 2300 [20].

$$Nu_D = C \cdot Re_D^{0.8} \cdot Pr_D^n \tag{4.17}$$

The variable n is 0.4 if the fluid is being heated, and 0.3 if the fluid is being cooled. The variable C is 0.021 for gases, 0.023 for non-viscous liquids, and 0.027 for viscous liquids [8]. The Reynolds number is computed as in 4.18.

$$Re = \frac{v_\infty \rho L}{\mu} = \frac{v_\infty L}{\nu} \tag{4.18}$$

v_∞ is the tube side fluid bulk velocity, ρ is the tube side fluid density in kg/m^3, L is the tube length, μ is the fluid dynamic viscosity in Pas and ν is the fluid kinematic viscosity in m^2/s. Equation 4.17 assumes that all fluid properties are evaluated at the arithmetic-mean bulk temperature, the Re-value should be above 10 000, and the Prandtl number should be between 0.7 and 100. The fraction of tube length and tube diameter, L/D, should be above 60. Moreover, there are some velocity constraints when considering shell and tube heat exchanger. Different velocity constraints can be viewed in table 4.2 [8].

Table 4.2: Velocity constraints of fluids of different phase and pressure in shell and tube heat exchangers [8]

Medium	**Velocity** $[\frac{m}{s}]$
Liquid (tube side)	1 to 4
Liquid (shell side)	0.3 to 1
Vapor (vacuum)	50 to 70
Vapor (high pressure)	5 to 10
Vapor (atm. pressure)	10 to 30

The Prandtl number, Pr, is computed as in 4.19.

$$Pr = \frac{\mu \cdot C_p}{k} \tag{4.19}$$

C_p is the heat capacity of the fluid in J/kg·K and k is the conductivity of the fluid in W/(m^3·K). Nusselt's correlation for finding the convective heat transfer coefficient can be seen in equation 4.20.

$$Nu = \frac{h_i \cdot d_i}{k} \tag{4.20}$$

where d_i is the tube inside diameter in meter.

For the convective heat transfer coefficient on the shell side, h_o can be computed from Nusselt's correlation as in equation 4.20, but with the hydraulic diameter d_e and the thermal conductivity k for the shell side fluid instead, as in 4.21.

$$Nu = \frac{h_o \cdot d_e}{k} \tag{4.21}$$

The hydraulic diameter d_e is the shell side equivalent diameter in meter. The calculations for d_e differ between different choices of tube arrangements. For a square pitch arrangement d_e can be computed via equation 4.22, and for triangular pitch it can be computed as in 4.23.

$$d_e = \frac{4 \cdot (\frac{p_t^2 - \pi \cdot d_o^2}{4})}{\pi \cdot d_o} = \frac{1.27}{d_o} \cdot (p_t^2 - 0.785 \cdot d_o^2) \tag{4.22}$$

$$d_e = \frac{4 \cdot (\frac{p_t}{2} \cdot 0.87 \cdot p_t - \frac{1}{2} \cdot \pi \cdot \frac{d_o^2}{4})}{\frac{\pi \cdot d_o}{2}} = \frac{1.10}{d_o} \cdot (p_t^2 - 0.917 \cdot d_o^2) \tag{4.23}$$

p_t is the tube pitch in m, and d_o is the outside tube diameter. The tube pitch is computed as in equation 4.24.

$$p_t = 1.25 \cdot d_o \tag{4.24}$$

To find the value of Nusselt's number, equation 4.25 can be used on the shell side.

$$Nu = j_h \cdot Re \cdot Pr^{1/3} \cdot (\frac{\mu}{\mu_w})^{0.14} \tag{4.25}$$

Re is computed via 4.18 where v_∞ is the shell side fluid velocity, μ is the shell side fluid dynamic viscosity, ρ is the shell side fluid density. Pr is computed as in 4.19 with properties for the shell side fluid. The fraction μ / μ_w is assumed to be equal to 1, as the viscosity at the wall and the fluid viscosity is similar in non-viscous fluids, as the ones considered in this thesis. This viscosity correlation factor is of greater importance in viscous liquids [8]. The j_h-factor can be read off a diagram depending on Re and L/D, or calculated via equation 4.26 for both tube- and shell side [8].

$$j_h = St \cdot Pr^{0.67} \cdot (\frac{\mu}{\mu_w})^{-0.14} \tag{4.26}$$

St is the Stanton number, computed in equation 4.27.

$$St = 0.0225 \cdot e^{-0.225 \cdot ln(Pr)^2} \cdot Re^{-0.205} \cdot Pr^{-0.505} \tag{4.27}$$

The fouling coefficients for the tube side and shell side, h_i and h_o, are tabular values that differ depending on the properties of the fluid [8]. Values of fouling coefficients for different fluids can be found in table 4.3 below.

Table 4.3: Fouling factors for different process fluids [8]

Fluid	**Fouling Coefficient** $\frac{W}{m^2 °C}$
Sea Water	1000-3000
Aquos Salt Solutions	3000-5000
Town Water	1000-5000
Organic Liquids	5000

These fouling factors are so-called dirt factors that affect heat transfer. Most process fluids have a fouling effect to a lesser or greater extent. Hence, it is important to design the heat exchanger to be oversized, to allow for some fouling. It is of course also necessary to have regular maintenance and cleaning of the exchangers to keep the fouling effects lower. The tabulated values over fouling coefficients are based on past experiences as they are difficult to predict.

For scenarios where the fluids change phase via vaporization, which occurs in the evaporator and generator, the heat of vaporization needs to be taken into account. Then pool boiling can be considered. Pool boiling takes place when a heated surface is submerged in a stagnant liquid and no external forced flow is applied. This means that motion in the relatively stationary liquid is driven by natural convection and bubble movement. The heat transfer coefficient h is computed from a different correlation of Nusselt's than regular heat transfer between two unchanged phases. This correlation can be viewed in 4.28 [8].

$$Nu = h \cdot \frac{(\frac{k_L^2 \cdot \sigma \cdot T_s^2}{h_{fg} \cdot \rho_v \cdot q^2})^{1/3}}{k_L} = \gamma \cdot 0.81 \tag{4.28}$$

σ is the surface tension in N/m, h_{fg} is the enthalpy of vaporization in J/kg, and q is the heat flux in W/m^2. γ is computed in equation 4.29 below.

$$\gamma = 0.28 \cdot (\frac{\rho_L}{\rho_L - \rho_V})^{1.73} \cdot \frac{d^{0.06} \cdot \rho_L^{0.05} \cdot h_{fg}^{0.04}}{a_L^{0.04} \cdot \rho_V^{0.03} \cdot \sigma^{0.02}} \tag{4.29}$$

a_L is the thermal diffusivity in m^2/s.

Another case is flow boiling, when a phase change occurs in a flowing fluid, for example on the tube side in shell and tube heat exchangers. For convective vaporization in boiling flow, Shah has developed a method to compute the heat transfer coefficient h that starts by computing the dimensionless numbers Bo (the boiling number), Co (the convection number) and Fr (the Froude number) seen in 4.30, 4.31, and 4.32 [8].

$$Bo = \frac{q}{G \cdot h_{fg}} \tag{4.30}$$

G is the total mass flow rate per unit cross sectional area.

$$Co = [\frac{1-x}{x}]^{0.8} \cdot [\frac{\rho_V}{\rho_L}] \tag{4.31}$$

x is the vapor fraction.

$$Fr = \frac{G^2}{\rho_L^2 \cdot g \cdot D} \tag{4.32}$$

D is the channel diameter.

Flow boiling is based on different regimes that evolves as the heat supply proceeds along the tube [8]. These regimes evolve from a single phase liquid to a bubble flow where small bubbles are formed, then a plug flow, slug flow, wavy flow, annular flow or drop flow and at last a vapor flow where the vapor fraction is 1. The plug flow, slug flow and wavy flow are names for how the gas bubbles become larger and larger as the flow is heated and evaporated. In the eventual gas phase, there are small liquid droplets carried along, and a liquid film will at first cover the channel walls. Eventually this liquid film will become gas, and then the heat transfer will decrease dramatically and the wall will become overheated. This phenomenon is called dry boiling, and is usually avoided when efficient heat transfer is required. However it is inevitable in evaporators if the fluid is being evaporated entirely. One more important thing to consider when calculating flow boiling in horizontal flows, is the negative pressure gradient formed in the direction of the flow as the fluid changes phase from liquid to gas. For vertical flows it is instead the density that affects the pressure gradient the most.

Due to the phase change occurring in flow boiling, a coefficient needs to be multiplied with the heat transfer coefficient. This multiplier, ψ, is the two phase multiplier for convective two phase heat transfer. ψ is depending on the boiling number, convection number and Froude number, as the flow boiling equations are a combination of nucleate boiling and convective vaporization. ψ is multiplied with the heat transfer coefficient for a single liquid phase h_L in order to obtain the heat transfer coefficient for a two-phase flow h_{tp}. This relation can be viewed in 4.33 [8].

$$\psi = \frac{h_{tp}}{h_L} = 15.43 \cdot Bo^{0.5} \cdot e^{\frac{2.47}{Co^{0.15}}} \tag{4.33}$$

Equation 4.33 assumes that Co$\leq$ 0.1 and Fr$\geq$ 0.04 for both vertical and horizontal tubes.

The single phase liquid heat transfer coefficient is computed via the Dittus-Boelter equation as in 4.34 [8].

$$h_L = 0.023 \cdot [\frac{G \cdot (1-x) \cdot D}{\mu_L}]^{0.8} \cdot Pr_L^{0.4} \cdot \frac{k_L}{D} \tag{4.34}$$

The index L stands for liquid, and the Prandtl number is computed as in 4.19. The two phase multiplier can then be read from a diagram depending on the boiling number and the convection number [8].

Computing the heat transfer coefficient for condensation means another relation than for evaporation is needed. This relation can be viewed in equation 4.35 [8].

$$h = 0.926 \cdot k \cdot (\frac{\rho_L \cdot (\rho_L - \rho_V) \cdot g}{\mu \cdot \Gamma})^{1/3} \tag{4.35}$$

This equation holds for condensation inside and outside vertical tubes, and Γ is the vertical tube loading in condensate rate per unit tube meter kg/(m·s) computed as in equation 4.36 [8].

$$\Gamma = \frac{W_c}{N_t \cdot \pi \cdot d} \tag{4.36}$$

d is either the inner or outer tube diameter, W_c is the total condensate flow, and N_t is the number of tubes in the bundle [8].

4.0.2.3 Shell and Tube Heat Exchanger Configuration and Design Choice

When designing shell and tube heat exchangers, there are several parameters that affect the design choice. To begin with, the tube dimensions should be chosen. Smaller tube diameters are preferred for most cases since it entails a more compact design and hence becomes cheaper [8]. However, if the process liquid allocated to the tube side is heavily fouling, larger tube diameters are favorable as they are easier to clean mechanically. If a much higher pressure is used within the tubes than on the shell side, it is favorable to have thicker tubes, also called gauge. Normal tube outside diameter is 16 to 50 mm, and normal gauge are 1.2 to 3.2 mm. Tube lengths normally vary from 2 meters to around 20 meters [21]. Typically, longer tubes entail smaller tube diameters, and this will reduce the heat exchanger cost [8]. The most optimal tube lengths usually lay in between 5 and 10 meters.

One way of increasing the tube length is to have tube passes. The number of tube passes also affect the tube side velocity and pressure drop. The normal number of tube passes vary between 1 and 16, and there are usually an even number of tube passes. Moreover, tube passes can potentially entail an internal temperature cross in the heat exchanger that can not be noticed from ΔT_{LM} in equation 4.12. Regarding the shell, the diameter usually varies in between 152 and 1524 mm according to the TEMA (Tubular Exchanger Manufacturing Association) standards [8]. The minimum shell thickness for carbon steel lays in between 7.1 and 9.5 mm. It is favorable to have a shell diameter that fits closely to the tube bundle to minimize bypassing along the shell. Depending on tube bundle type, such as U-tube, packed head or floating head, there are different recommendations

for shell-bundle clearance. The size of the tube bundle depends on the number of tubes and the number of tube passes, as well as the tube diameters. The number of tubes can be computed as in equation 4.37.

$$N_t = K_1 \cdot (\frac{D_b}{d_o})^{n_1} \tag{4.37}$$

where N_t is the number of tubes, K_1 and n_1 are constants depending on the tube arrangement and number of tube passes that can be found in tables, and D_b is the tube bundle diameter. D_b is further computed as in equation 4.38.

$$D_b = d_o \cdot (\frac{N_t}{K_1})^{\frac{1}{n_1}} \tag{4.38}$$

Moreover, the tubes can be configured in different ways, and there are three configurations that are the most common ones: triangular pitch, square pitch and rotated square pitch [8]. Triangular pitch and rotated square pitch generally give higher rates of heat transfer, but the square pitch gives a lower pressure drop. Usage of heavily fouling process fluids on the shell side benefit from using a square or rotated square pitch as it simplifies cleaning. The tube pitch is commonly $1.25 \cdot d_o$.

The shell can also be designed in a multitude of ways in relation to the tube bundle [8]. The most common and also cheapest configuration is to have a fixed tube sheet where the tube bundle is non-removable. However, in order to simplify cleaning, which is necessary for heat exchangers operating with fouling liquids, a floating head, with removable tube bundle could be a good choice. A floating head shell with removable tube bundle also allows for differential expansion of the shell and tubes if they for example are made out of different materials and expand at different temperatures. Hence, the floating head heat exchanger is optimal if operated at large temperature differences. However, this configuration requires a larger space between the tube bundle and shell. This space, called the shell-bundle clearance, can be optimized from diagrams for different shell types, and it typically ranges between 10 and 100 mm. Another common shell type are U-tubes or U-bundle, which are cheaper than the floating head shells, but are much more difficult to clean.

The materials considered for the AHT are carbon steel in the equipment where LiBr is not used, and stainless steel 316 where LiBr is present. This is because LiBr in an aqueous solution is corrosive as said in section 4.0.1.3, especially when it undergoes reactions 4.5 to 4.8 where solid salt can be formed.

4.0.3 Cost Calculations

In order to evaluate whether a project is worth implementing or not, the cost needs to be computed. The total cost of a project does not only include the cost of the equipment in terms of material and fabrication, but also includes engineering hours, piping costs, potential buildings and reconstructions of the ground. Also, as total investment cost calculations have a lot of uncertain parameters, a contingency factor is commonly added to account for unexpected costs thar arise as the project progresses. In order to evaluate the project, the revenues also need to be considered. The evaluation is later based on how long it will take to pay the investment back, and how much money can be saved by implementing the project. Companies usually have an internal threshold for the backpack period to invest in them. This threshold varies, but about 3.5 years is common in the petrochemical industry [22].

4.0.3.1 Investment Cost and Evaluation Methods

The material cost for most industrial equipment can be computed via equation 4.39 [23]. The variables a, b and n varies depending on material and type of equipment. The variable S is the parameter determining the size of the equipment, which in turn affects the cost. For a heat exchanger for instance, S is the area in m^2, and for a pump, S is the capacity in L/s.

$$C_e = a + b \cdot S^n \tag{4.39}$$

Where the parameters a, b and n are constants used to compute the costs [8]. In the table, all costs are for equipment made in carbon steel, and additional factors can be multiplied by the cost in order to calculate for other materials. For instance, for stainless steel 316 this factor is 1.3 [23]. An additional installation factor, a so called Lang factor, can also be multiplied to the equipment cost in order to compute the investment cost. The Lang factor covers the cost of the plant it self, the ISBL, which includes producing and installing, the process equipment, delivering cost as well as engineering costs. The Lang factor has different values depending on which process is considered. In table 4.4 Lang factors for different processes can be viewed.

Table 4.4: Lang factors for different processes [8]

Process	**Lang factor**
Solids processing plants	3.1
Fluids processing plants	4.74
Mixed solids and fluids processing plants	3.63

Other additional costs that need to be taken into consideration are piping costs. These are computed with respect to the pipe length and diameter, as well as material. To calculate the cost of pipes, equation 4.40 can be used in case the pipes are made out of carbon steel [24].

$$C_{pipe} = (d_o - d_w) \cdot d_w \cdot 0.02466 \cdot c_m \cdot L \tag{4.40}$$

C_{pipe} is the pipe cost in SEK, d_o is the tube outside diameter in m, d_w is the wall thickness of the tube wall in m, c_m is the cost per mass of carbon steel in SEK/kg, and L is the tube length in m [24]. Wall thicknesses for different tube diameters, and the corresponding price per mass of carbon steel pipes can be found in tables [25].

To evaluate whether the investment is financially beneficial, the Pay Back Period (PBP) can be computed as in 4.41 [23].

$$PBP = \frac{Total\ Invenstment}{Average\ Annual\ Cash\ Flow} \tag{4.41}$$

Another way of evaluating the investment is via the Net Present Value (NPV) showen in equation 4.42. The NPV is the sum of the present values of the future cash flow, meaning it represents the difference between the present value of cash inflows and the present value of cash outflows over a period of time. If the NPV has a value greater than 0, it indicates that the investment will be profitable since it generates more money than it costs. A NPV equal to 0 indicates the investment is expected to break even, and an NPV less than 0 means that the investment will cost more than it generates. The NPV value was computed for year one to 20, as this commonly is the depreciation period, when the economic value of an equipment at last becomes insignificant.

$$NPV = \sum_{n=1}^{n=t} \frac{CF_n}{(1+i)^n} \tag{4.42}$$

CF_n is the cash flow in year n, i is the interest rate and t is the project life in years. The interest rate is considered to be 10% in this work.

Finally, the annual net profit (ANP) can also be used to evaluate the investment. The ANP relation computes the remaining value after the total expenses of an investment with revenue [23]. As for the NPV, the value 20 years after the investment is regarded.

$$ANP = CF - r \cdot i \tag{4.43}$$

4.0.3.2 Revenue Calculations

The sources of income in this work are the decrease in carbon dioxide emissions, the water intake savings, and reduction in fuel gas use. The carbon dioxide emissions can be calculated with the fuel gas flows by knowing the molar ratio between CH_4 and CO_2 as in 4.44.

$$\dot{m}_{CO_2} = \frac{M_{CO_2}}{M_{CH_4}} \cdot \dot{m}_{CH_4} \tag{4.44}$$

$\dot{m}$ is the mass flow in kg/s, and M is the molar mass in kg/kmol. The reduction in carbon dioxide emissions can hence be computed via the same equation, knowing how large the reduction in mass flow of fuel gas is. One way of calculating this is by knowing how much the fresh water intake can be reduced, and using relation 4.45.

$$\dot{m}_{fg,\ save} = \frac{(H_{vap} + (h_{p,T,sh} - h_{p,sat.\ vap}) + (h_{p,\ sat.\ liq} - h_{p,\ sat.\ liq})) \cdot \dot{m}_{water\ save}}{\eta_{boiler} \cdot HV_{eff}} \tag{4.45}$$

$\dot{m}_{fg,\ save}$ is the mass flow of fuel gas reduction in kg/s, H_{vap} is the heat of vaporization, h is the enthalpy of water at different conditions in kJ/kg, $\dot{m}_{water,\ save}$ is the mass flow of saved water intake in kg/s, η_{boiler} is the boiler efficiency assumed to be 85%, and HV_{eff} is the effective heating value of fuel gas in kJ/kg.

The fuel gas losses from using quench oil for the AHT instead of preheating water into the cracking furnaces is computed below in equation 4.46.

$$\dot{m}_{fg,\ totsaved} = (\dot{m}_{fg,\ save} - \frac{P_{quench}}{HV_{eff} \cdot \eta_{furnaces}} \cdot t) \tag{4.46}$$

$\dot{m}_{fg,\ totsaved}$ is the total fuel gas reduction in kg/h, $\dot{m}_{fg,\ save}$ is the fuel gas saved from removing one boiler in kg/h, P_{quench} is the effect of the quench heat loss in kW, HV_{eff} is the effective heating value of the fuel gas in kJ/kg, $\eta_{furnaces}$ is the furnaces efficiency assumed to be 85%, t is the yearly operating time in h.

The money saved for the fuel gas reduction can be based on the price of natural gas, that is added as makeup to the fuel gas in order to supplement it out. The reduction in cost of fuel gas when implementing the AHT can hence be based on the reduction in makeup used. The reduction in CO_2 emissions can be computed as in 4.47. M_{CO_2} is the molar mass of carbon dioxide, and M_{CH_4} is the molar mass of methane in kg/kmol.

$$\dot{m}_{CO_2,\ save} = \dot{m}_{fg,\ save} \cdot \frac{M_{CO_2}}{M_{CH_4}} \tag{4.47}$$

The combustion of CH_4 which generates CO_2 can be seen in reaction 3.1. The final revenue can be computed as in 4.48.

$$R_{CO_2} = \dot{m}_{CO_2,\ save} \cdot C_{CO_2} + \cdot m_{fg,\ save} \cdot C_{fg} \tag{4.48}$$

R_{CO_2} is the revenue from decreasing the consumption of fuel gas and the reductions of carbon dioxide emissions in SEK, and C_{CO_2} is the cost of emitting one tonne of carbon dioxide in SEK/(kg CO_2) and C_{fg} is the cost for fuel gas in SEK.

Moreover, looking at the reduced water intake, the savings can be computed as in 4.49.

$$R_{water} = \dot{m}_{water,\ reduced} \cdot t \cdot P_{water} \tag{4.49}$$

R_{water} is the fresh water reduction revenue in SEK, $\dot{m}_{water,\ reduced}$ is the mass flow of reduced fresh water intake in ton/h, t is the operating hours per year, and P_{water} is the price of freshwater in SEK/ton. The reduction in mass flow of fresh water is the same as amount of regenerated DS.

The cost of HP steam can be related as in 4.50.

$$C_{HP} = \dot{m}_{HP} \cdot t \cdot P_{HP} \tag{4.50}$$

P_{HP} is the price of HP in SEK/ton, t is the operating time in hours per year considered to be 8300 h/year, and $\dot{m}_{HP}$ is the mass flow of HP used.

HP steam is currently used in a turbine to produce electricity by expanding HP steam to MP steam. There will therefore also be a loss in electricity production as HP steam is used for producing DS instead of being expanded. Less HP steam will hence be produced since DS steam is produced of the stripper flow instead. This loss in electricity generation can be computed as in 4.51.

$$Q_{turbine} = (h_{in} - h_{out}) \cdot (\dot{m}_{HP} + \dot{m}_{water}) \tag{4.51}$$

h_{in} is the enthalpy for superheated HP steam at 86 bar and 480°C, and h_{out} is the enthalpy of MP steam at 280°C and 9.8 bar, both measured in kJ/kg.

The electricity consumption can be computed as in 4.52.

$$C_{el} = (\sum Q_{pump}) \cdot t \cdot P_{el} \tag{4.52}$$

C_{el} is the cost of electricity in SEK, $\sum Q_{pump}$ is the sum of all pump work in kW, t is operation time i hours, and P_{el} is the electricity price in SEK/kWh.

4.0.4 Pressure Drop Calculations

In all equipment included in an AHT, there will be pressure drops as it consists of shell and tube heat exchangers [20]. Of course there are also pressure drops in the pipes that need to be considered. The two main factors causing a pressure drop is friction on the fluid from the channel walls, and losses caused by contractions and expansions in the channel [8]. In the AHT, it is important to keep the original pressures for the process, as the water stream and LiBr-solution stream evaporates and condenses at specific temperatures at certain pressures. There is a pump and a pressure valve in the AHT LiBr-cycle that can be used to adjust the pressures. The pump downstream the preheater can be used to obtain the right pressure in the absorber, taking pressure drops in the preheater and evaporator into account.

The pressure drop in the heat exchanger on the shell side was computed via equation 4.53 [8].

$$\Delta P = 8 \cdot j_{f,shell} \cdot \frac{d_{shell}}{d_o} \cdot \frac{L}{D_B} \cdot \frac{\rho \cdot v^2}{2} \cdot (\frac{\mu}{\mu_w})^{-0.14} \tag{4.53}$$

The value -0.14 is set assuming that Reynolds number is above 2100 [8]. If the Reynolds number would be less than 2100, a value of -0.25 should be used instead. ΔP is the pressure drop in Pa, $j_{f,shell}$ is the friction factor on the shell side depending on baffle arrangement and Reynolds number, d_{shell} is the shell diameter in m, d_o is the tube outside diameter in m, L is the shell length in m, D_B is the baffle spacing computed in equation 4.54, ρ is the shell side fluid density in kg/m^3, v is the shell side fluid velocity in m/s, and μ/μ_w is the dynamic viscosity in the fluid divided by dynamic fluid viscosity at the tube wall [8]. This fraction is approximated to be one in this work.

$$D_B = 0.5 \cdot d_{shell} \tag{4.54}$$

On the tube side, the pressure drop is computed via formula 4.55 [8].

$$\Delta P = n_t \cdot (8 \cdot j_{f,tube} \cdot \frac{L}{d_i} \cdot (\frac{\mu}{\mu_w})^{-0.14} + 2.5) \cdot \frac{\rho \cdot v^2}{2} \tag{4.55}$$

d_i is the tube inside diameter and N_t is the number of tubes. The number 2.5 comes from Frank's method of estimating pressure losses [8].

In order to calculate pressure drops in the pipes, equation 4.56 was used, that is Bernoulli's equation with head losses [20].

$$\Delta P = \rho \cdot (g \cdot \Delta h \cdot \frac{v_2^2 - v_1^2}{2} + \Sigma h_L \cdot g) \tag{4.56}$$

The sum of all head losses and flow losses is the head loss Σh_L. Head losses consist of pipe bends, tapers and such, while flow losses consists of streaming losses due to friction on the tube walls. Only 90°pipe bends are used in this work. Head losses due to flow losses is calculated as in 4.57, while head losses are computed as in 4.58 [20].

$$h_L = 2 \cdot f_f \cdot \frac{L}{d} \cdot \frac{v^2}{g} \tag{4.57}$$

$$h_L = K \cdot n_{bend} \cdot \frac{v^2}{2 \cdot g} \tag{4.58}$$

f_f is the fanning factor that can be read from a diagram with respect to the Reynolds number and the fraction ε/d where ε is the pipe roughness, in other words how much the unevenness of the pipe surface measured in meters, an d is the pipe diamter. K is a value that can be taken from a table, depending on how the pipe is bent, n_{bend} is the number of pipe bends [20].

Some general pressure drop limits considered is a maximum of one bar on both the shell and tube side in shell and tube heat exchangers [8]. However, in an AHTs the generator and condenser operate at comparatively low pressures, the pressure drops in this equipment need to be carefully handled to prevent absolute vacuum.

4.0.5 EU Emission Trading System

The European Union (EU) launched the EU emissions trading system *EUETS* in 2005 to help reduce emissions of green house gases *GHG* while at the same time generate revenue for a green transition [26]. A limit has been set on the maximum allowed emissions of GHG. This limit is expressed as allowances where one allowance corresponds to the right to emit one tonne of CO_2 *equivalents*. The limit, or *cap*, is reduced annually to ensure a reduction of the GHG emitted. The EU ETS covers the heat and energy sector, industrial manufacturing, aviation sector as well as maritime transportation. Companies are either assigned a certain allowance or have to buy them. This generates a market where companies have to buy enough allowance to account for the total amount of emissions for the whole year otherwise they are subjected to heavy fines. The cost of an allowances for one ton of CO_2-eq was 84 € in January 2025, and reached an all time high of 105 €/tonne in March 2023 [27].

4.0.6 Safety Risks

In this subsection, safety risks of the chemical compounds involved will be described.

Lithium Bromide (LiBr)

Crystalline LiBr has acute oral toxicity, causes skin irritation, severe eye damage, and skin sensitization [28]. Personal protective equipment should be used when handled, and releasing it to the environment should be avoided.

Lithium Molybdate

Lithium molybdate is irritating to the skin and eyes and toxic to organs [29]. Moreover, it is very hazardous to ingest. In case of fire, lithium molybdate forms hazardous compounds such as lithium oxides and molybdenum oxides.

Ethylene Glycol

Ethylene glycol is harmful if ingested and can cause damage to organs [30]. Contact with skin, eyes, and clothes should be avoided. Protective clothes should be therefore worn when handling the compound. Regarding flammability, ethylene glycol is combustible but will not ignite readily.

Phenols

Phenols are acutely toxic through inhalation, dermal, and oral exposure[31]. It causes irritation to skin and eyes and can lead to severe eye damage. Moreover, phenols can entail chronic hazards when exposed in aquatic environments. Lastly, it can cause germ cell mutagenic damage and be toxic to organs if exposed repeatedly.

Overhead process Fluid and Quench Oil

The overhead process stream and quench oil consists of a mixture of various hydrocarbons. Inhalation, aspiration or ingestion of hydrocarbons can be very toxic and even lethal [32]. This can be a potential risk as some hydrocarbons are volatile and hence easily inhaled. Leakage of hydrocarbons that come in contact with air could cause fire or explosion [33].

Pressure Risks

High pressures in industrial equipment could cause explosions and constitute safety risks for workers [34]. Some examples of potential hazards are leakages of hot steam, blasts from explosions leading to flying debris from equipment being torn apart, and fire. These risks due to pressure depend on the process fluid and amount of stored energy [35]. The *Pressure Equipment Directive* requires that all pressurized equipment operating above 0.5 bar are controlled, and that it is made sure that it is safe to operate before implemented in a process.

5
Methods

In this section, the procedure leading up to the final design will be described in detail. To begin with, the procedure of investigating how much DS can be generated by the waste heat was carried out testing a CCC, MVR and AHP. Thereafter, the method of investigating the AHT will follow with a more detailed description. Firstly, it will be described how the design was found and simulated, and thereafter it will be described how the cost and sizes were computed. Lastly, it will be explained how the sensitivity analysis was carried out.

The waste heat available in the overhead is 65 MW and 13 MW in the quench oil. The overhead consists of a mixture of water, light hydrocarbons and heavy hydrocarbons, while the quench oil consists of heavy hydrocarbons in liquid phase. The water stream that could be generated to DS is either the stripper flow or the BET flow. The properties of these streams are found in table 5.1 below.

Table 5.1: Properties of the streams available in this work.

Stream	Temperature [°C]	Pressure [bar]	Mass flow [$\frac{ton}{h}$]
Stripper	110	4	100
BET	30	1	110
Overhead	112 - 34	1.25	360 000
Quench oil	187 - 161	7	1 402 885
HP	480	86	-
DS	240	9.8	-

5.0.1 Simulation of CCC Heat Pump

When investigating the CCC heat pump, it was considered that the DS steam was needed to be produced from water purer than the stripper water. This was before it had been realized that the stripper water was pure enough. Therefore, it was considered that the DS was to be generated from the water cleaned by the BET. This water, at 30 °C, is much colder than the stripper water of 110 °C.

A CCC heat pump requires a refrigerant. Hence, a literature study of different refrigerants was performed, where five refrigerants considered to be efficient were simulated. The results from these simulations can be observed in table A.1 in Appendix, section A.

The evaporator was simulated as a plate heat exchanger in Aspen Hysys. This choice of heat exchanger type was mainly to avoid F-factor correlation errors, which shell and tube heat exchangers are more sensitive to. The outlet pressure in the compressor was set in order to receive the desired temperature lift, of a temperature above 240 °C in order to generate DS from the BET or stripper outlet. The condenser was also simulated as a plate heat exchanger, where the compressed working

fluid was either heat exchanged with the BET water or the stripper outlet stream. The working fluid is then recirculated back to the evaporator, and in order to have the same ingoing pressure and temperature, a pressure throttle and sometimes a cooler was used.

5.0.2 Simulation of MVR Heat Pump

Another configuration considered was a MVR heat pump, which is an open heat pump that directly heats and compresses the water to DS. Simulations of the MVR were performed in Aspen Hysys, and the configuration generally consisted of only an evaporator and a compressor. The evaporator was represented by a plate heat exchanger, since this type allowed a broader range of temperature differences. The shell and tube heat exchanger is more sensitive to F-factor violations as it is not truly countercurrent.

Several different MVR configurations were tested and simulated in Hysys. Two simulations were preformed where the overhead from 112 to 35 °C was used, as well as only from 112 to 58 °C to preheat and evaporate the water from the BET. The vapor was then compressed to achieve the right temperature and pressure. It was noticed that by compressing the evaporated water, the temperature would become very hot when the desired pressure was obtained. This problem was solved by injecting cold feed-water to the compressor outlet: a commonly used technique called de-superheating. The water injection was more efficient than implementing a cooling heat exchanger to obtain the right temperature. This because the flow increases by cool water injection but the compressor work is unaffected.

Another solution for generating DS from the BET flow was to have a HP steam injection prior to the compression instead of an evaporator. However, evaporation with HP steam required a very high flow, meaning the freshwater reduction would be less for the same amount DS generated. Therefore a pump was needed prior to the compression to increase the pressure without increasing the temperature. Other configurations assessed were having two compressors in series with intermediate water injection, and to have intermediate cooling via heat exchangers between two compressors.

For the last configuration for the BET, it was also tested whether it would be favorable to use HP steam in the evaporating heat exchanger prior to the compression instead of injecting the steam directly. MVR simulation attempts are compiled in table A.2 in Appendix, section A.

On the other hand, if the water needed for MP steam production does not have requirements of being purified in the BET, it would be a better alternative to utilize the liquid bottom outlet from the stripper tower and generate steam from it directly. This is since the stripper outlet is much warmer than the water in the BET, that is cooled when it undergoes purification.

Since the furnaces contain a mixture of hydrocarbons, the fact that the stripper water contains at most 50 ppm phenols will not lead to a contamination in the cracking process [36]. However, 50 ppm of phenols means 50 tonnes/h in the DS flow. As the water evaporates at the DS properties, the phenols can crystallize and contribute to fouling. However, in the following heat pump configurations, the fouling possibilities were disregarded.

One possible solution for generating DS from the stripper outlet could be to use excess heat from quench oil heat exchangers used for preheating water for steam production. This heat, with temperatures from 187 to 161 °C, could be used to heat and evaporate the stripper outlet stream of 110 °C. This was tested in Aspen Hysys. It resulted in a configuration where the stripper outlet first was pressurized to 9.8 bar. Then the quench oil evaporated the stripper outlet at 179 °C, whereupon HP steam was used to superheat it to 240 °C. This solution can be viewed in Appendix A in table A.2.

5.0.3 Simulation of AHP

Another concept investigated was using an AHP with LiBr and water as working fluids. This simulation was made using the overhead waste heat stream to evaporate the working fluid of LiBr dissolved in water. In an AHP, the working fluid was thereafter absorbed, whereupon it was pumped up to a generator. In the generator, steam was added to evaporate the working fluid. The mechanism in the evaporator was to have a pressure low enough to make the working fluid evaporate at a lower temperature. The pressure set in the absorber was 0.04 bar, which made the working fluid boil at 96 °C. After the absorption, the working fluid is pumped up to 8 bar, where is is evaporated in the generator at 180 °C. This heat is thereafter used for heating the stripper outlet from 110 °C to 160 °C at 5 bar. The condensed working fluid is thereafter throttled back to the low evaporator pressure of 0.04 bar. The stripper outlet is heated to 160 °C and is fully evaporated, but does not meet the temperature and pressure requirements of DS. Therefor it is compressed to 9.8 bar afterwards.

5.0.4 AHT

It was further investigated whether an AHT could be an appropriate equipment for the purpose considered. In this case, the overhead waste heat together with the quench oil is considered as the medium temperature heat source, and the goal would be to lift the temperature to over 179 °C, that is required to evaporate the stripper outlet at 9.8 bar. This since no compression would in this case be needed, only superheating of the generated steam. A low grade stream will also be generated from the AHT.

5.0.4.1 Requirement of an AHT

The sought after outcome of the AHT is to procedure DS at 9.8 bar. The saturation temperature of water at 9.8 bar is 179 °C [37]. To evaporate the water from the stripper, the temperature in the absorber thereby needs to be at least 189 °C if a minimum temperature difference for the heat transfer of 10 °C is wanted.

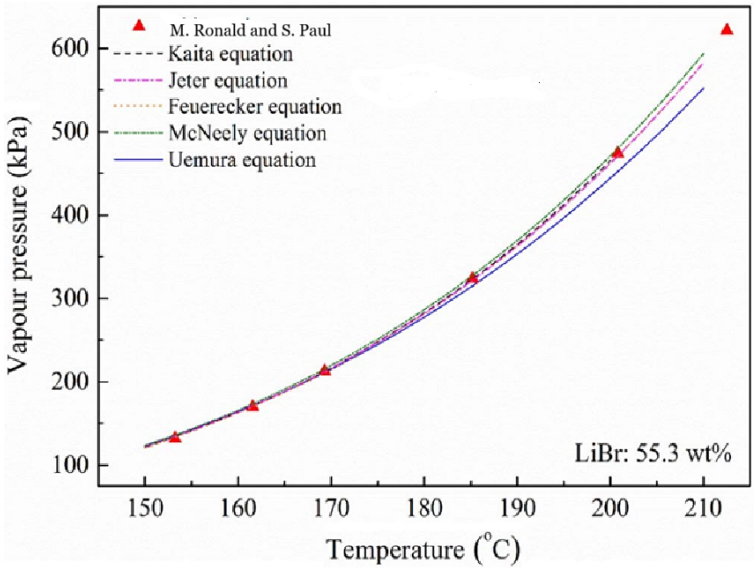

Figure 5.1: Saturation temperature of LiBr in an aqueous solution [38].

As can be seen in figure 5.1, if a temperature of 189 °C or above is wanted in the absorber, a vapor pressure of about 4 bar or more is needed. Water at 4 bar evaporates at 144 °C and at 5 bar at

153 °C [37]. Since the absorber and evaporator operate at the same pressure the heat source in the evaporator needs to be of a least 154 °C (144 °C plus ΔT_{min} of 10 °C). The heat source in the evaporator thereby can not be the overhead since its temperature is between 112-35 °C, instead the quench oil of 187 °C has to be used.

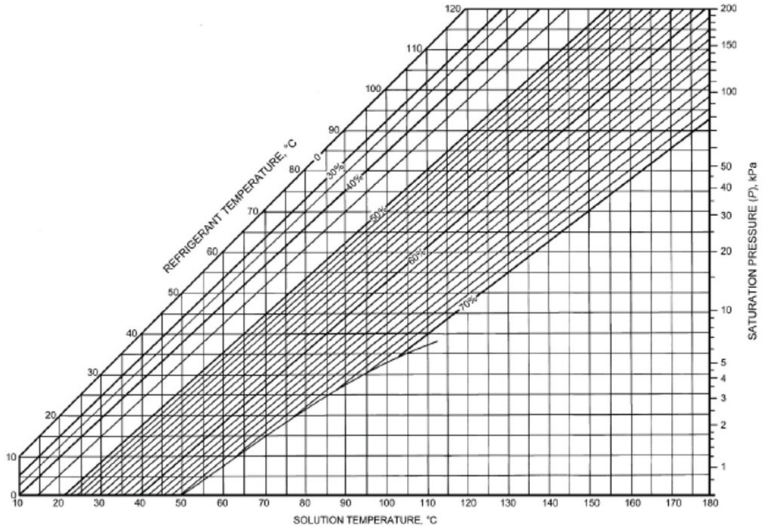

Figure 5.2: Saturation temperature of LiBr in an aqueous solution at lower temperatures [39].

To regenerate the water vapor in the generator a heat input is needed. If this heat source is to be heat from the overhead, the temperature in the generator needs to be less than 102 °C (the overhead is 112 °C minus a ΔT_{min} of 10 °C) which would indicate a pressure of less than 15 kPa (0.15 bar) as can be seen in figure 5.2. The generator and condenser operates at the same pressure. Water at 0.15 bar condenses at 53 °C [37].

Since the waste heat sources (the overhead and quench oil) have a limited temperature range, the design and choice of operating pressures in the AHT becomes limited as well since the pressure affects the condensation and evaporation temperatures of the working fluid, which have to match the temperatures of the input heat.

5.0.4.2 Simulation of AHT

The simulation of the AHT was conducted in Aspen Plus, as Hysys does not allow dissolution of salts and electrolytes. The working fluid considered was water and an aqueous solution of LiBr. The two most common working fluid pairs are LiBr and water and ammonia and water. Since the heat output in the AHT is in the absorber, a temperature of 179 °C in it is needed. To accomplish this a working medium with the right properties is required. Water has a boiling point of 10 0°C at 1 bar while ammonia has a boiling point of -33 °C at 1 bar. The boiling point of ammonia is too low to be able to be absorbed at such high temperature and therefore it is unsuitable for this application. Hence, water-LiBr was was chosen as the working pair. The working pair LiBr-water however has some drawbacks named in section 4.0.1.3, entailing that the process needs maintenance. Despite this, this solution was the obvious choice due to the boiling points. Moreover, ethylene glycol and lithium molybdate were added to the LiBr-water solution to reduce corrosion and increase the efficiency of the heat pump. The lithium molybdate should not influence the performance of the AHT. This was made sure by adding 100 ppm of lithium molybdate to the LiBr-solution to the AHT-simulation in Aspen Plus, where it was confirmed that it had no influence on performance. Ethylene glycol was added to the LiBr-solution with a weight ratio of 1:4.5 LiBr solution.

In Aspen Plus, the AHT was simulated by shell and tube heat exchangers representing the preheater and evaporator, an equilibrium reactor and shell and tube heat exchanger representing the absorber, a shell and tube heat exchanger representing the solution heat exchanger, a simple separator representing the generator, and a shell and tube heat exchanger representing the condenser. The simulation can be viewed in figure 5.3 Moreover, one last heat exchanger was used to superheat the generated steam to the right temperature of DS.

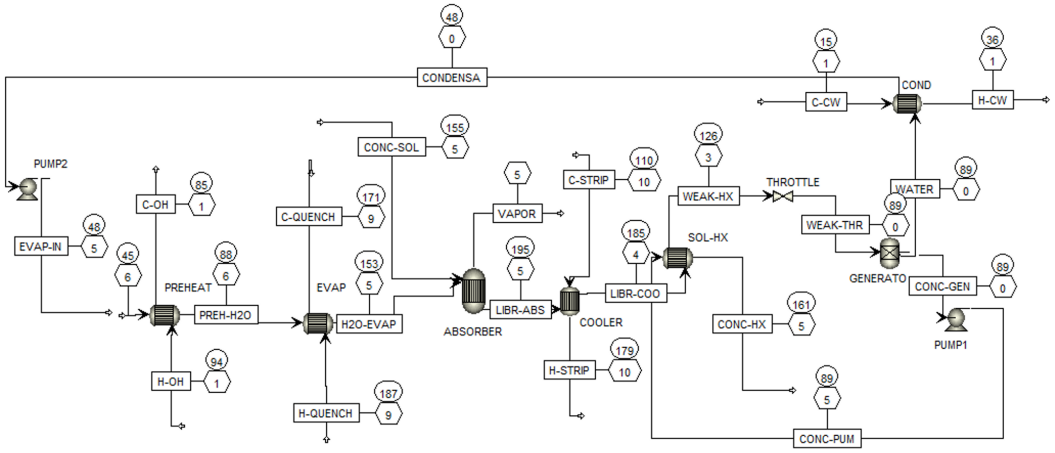

Figure 5.3: AHT simulation in Aspen Plus. Temperature can be viewed in the circles in °C, and pressure is visualized in the hexagons in bar.

The heat inputs into the AHT are located at the preheater, evaporator and generator. In the generator, the waste heat from the overhead was used from 112 °C to 94 °C. Here the entire flow of 360 ton/h of the overhead was utilized. The preheater used heat from the overhead from 94 to 87 °C, but only required 120 ton/h of the total flow. The evaporator uses heat from the quench oil from 187 to 171 °C, with a mass flow of 100 ton/h.

The AHT was simulated as a single-stage heat transformer. However, other configurations with two stages were also tested in Aspen Plus. The two-stage AHT uses the heat generated in the absorber as the medium temperature heat source in the next cycle. In this way the temperature can be lifted two times and could reach higher temperatures at the end. However, with the right pressures and temperatures, and by utilizing all waste heat available from the overhead and quench heat exchangers, one AHT cycle was found to be enough to enable heating and evaporating of the stripper outlet to approximately 180 °C. A single stage AHT will have a higher COP than a two stage AHT and the single stage one was therefore chosen.

The fluid package used in Aspen Plus was the ELECNRTL as ions were involved. It was set so that no salt formation were allowed in the Elec Wizard tool, but aqueous solutions of salt were allowed. This was done to avoid handling solid compounds in Aspen Plus. Also, as the concentration of LiBr to water was within the solubility limits, it was assumed that no solid forms of salt were formed.

Preheater

The first unit in the AHT cycle was the preheater, that is the first heat exchanger from the left in figure 5.3. It can be viewed separately in figure 5.4 in more detail. This was simulated as a shell and tube heat exchanger with the overhead flow on the shell side and water on the tube side. The

purpose of the preheater is to utilize waste heat to heat the water before evaporating it, so that less energy will be needed for the evaporation. With an overhead flow of 120 ton/h, the water flow of 19.4 ton/h could be preheated to 88 °C. The flow of 19.4 ton/h is a value that was iterated with respect to the heat input in the generator in order to regenerate the same amount of water.

Evaporator

After being preheated, the water enters the evaporator, where heat from quench oil is utilized to evaporate it. This is simulated as a shell and tube heat exchanger in Aspen Plus, with the quench oil on the tube side and water on the shell side according to the fluid allocation recommendations in section 4.0.2.3. The evaporator is the second heat exchanger from the left in figure 5.3, named *EVAP*. It can also be viewed in figure 5.5 in more detail. A quench oil mass flow of 1402.8 ton/h was used to evaporate 19.4 ton/h water at 5 bar, where the saturation temperature is 151.85 °C. The outlet temperature of the water vapor was 153 °C.

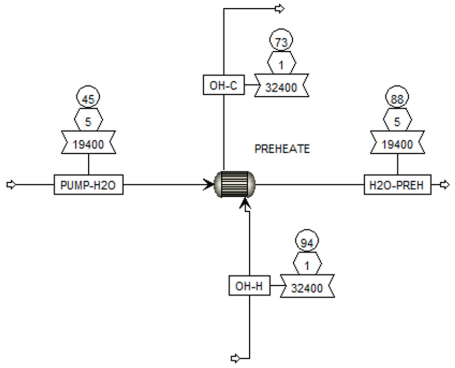

Figure 5.4: Simulation of the preheater in Aspen Plus. The temperature is showed in the circles in °C, the pressure is showed in the hexagons in bar, and the rectangles show the mass flow in kg/h.

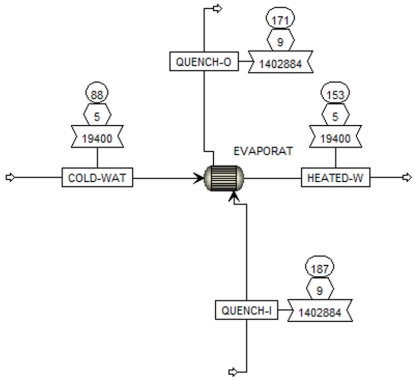

Figure 5.5: Simulation in Aspen Plus over the evaporator. The temperature is showed in the circles in °C, the pressure is showed in the hexagons in bar, and the rectangles show the mass flow in kg/h.

Absorber

The absorber was simulated as an equilibrium reactor in Aspen Plus, visualized in figure 5.3 with the reactor named *ABSORBER*. The reactions 4.5, 4.6, 4.7 4.8, and 4.9 are taking place in the absorber. Reaction 4.7 is the autoprotolysis of water that occurs as a side reaction, the formation of H_3O^+ and OH^- occurred at such a small extent that their presence was neglected. Reaction 4.8 is the dissociation of LiBr. In this work, it is however considered that the LiBr salt is already dissolved in water as ions when it enters the AHT as a concentrated LiBr-solution. The concentrations of the solution were: of 56.12 wt-% of LiBr, 34.99 wt-% water, and 8.89 wt-% etylene glycol. This ratio is within the solubility range at 195 °C and 5 bar, which can be seen in figure 5.1. So, reaction 4.8 takes place before entering the AHT, and reactions 4.5, 4.6 and 4.7 occurs to a very small extent in the reactor. It is hence reaction 4.9 that is the most important reaction in the absorber. The LiBr concentrations decreased from 56.12 wt-% to 51.35 wt-%, while the water mass concentration increased from 34.99 wt-% to 40.49 wt-% during the reaction. All these ratios are within the solubility range which can be controlled in figure 5.1.

There are two streams entering the absorber on the shell side, the concentrated LiBr-solution stream and the water vapor stream. The concentrated LiBr-solution holds 153 °C and 5 bar, and

so does the water vapor stream. As reaction 4.9 takes place, the temperature rises to 195 °C in the reactor. Heat from the reaction is transferred to the stripper water flowing through the tubes and the stripper water is fully evaporated. The reaction will heat the LiBr solution to 195 °C and the solution will cool down as it flows down the tubes in the absorber. However, the reactor was only possible to simulate at a constant temperature. Therefore, a cooler simulated by a shell and tube heat exchanger was implemented following the equilibrium reactor, named *COOLER* in figure 5.3. So as reactions 4.5, 4.6, 4.7 and 4.9 took place, a constant temperature of 195 °C was maintained. In the following cooler, the weak LiBr-solution heated the stripper flow and the temperature of the solution decreased from 195 to 185 °C. These two units together represented the absorber.

The stripper becomes steam at 182 °C and 9.8 bar, 3 °C superheated. There is at most 50 ppm phenols in the stripper flow, as the concentration is so low it was assumed that the stripper flow had the properties of pure water. The heat released in the reactor unit was 7083.92 kW and the following cooler had a heat duty of 1645.64 kW.

In order to check whether this simulation was representative of a real absorber, a back-of-an-envelope-calculation was performed where the heat from condensing 19.4 ton/h of water vapor was computed. This was done by multiplying the heat of vaporization at prevailing conditions in kJ/kg with the mass flow in kg/s. The heat required for heating the concentrated LiBr-solution from 153 °C to 195 °C was then subtracted. This heat was approximately the same as the heat duty in the reactor. Most of the heat from the reaction originates from the condensation of the water vapor as it is absorbed and should therefore be the same.

Solution Heat Exchanger

The next unit, the solution heat exchanger, was simulated by a shell and tube heat exchanger in Aspen Plus, where the weak LiBr-solution exiting the absorber was the hot stream going on the shell side, and the cold concentrated LiBr-solution exiting the generator went on the tube side. The solution heat exchanger is visualized as *SOL-HX* in figure 5.3. The purpose of this exchanger's is to preheat the concentrated LiBr solution before it enters the absorber again, and simultaneously cool the weak LiBr-solution before it entered the generator at a lower pressure. To adjust the pressures, a valve and a pump were used. The valve took the pressure down from 5 to 0.1265 bar before the generator, and the pump took it back to 5 bar after the generator.

The solution heat exchanger later had to be designed as two separate units, as using only one unit caused a temperature cross. It is however simulated as one unit in the AHT in Plus, as Plus does not take heat exchanger design into consideration. It was however separately designed as two, in order to get a more detailed picture of how it could be designed and what the operating conditions would be. This can be viewed in figure 5.6. The reason another type of heat exchanger than shell and tube was not considered when designing and sizing the solution heat exchanger, was that shell and tube heat exchangers are very common in chemical industries as they are relatively cheap and easily cleaned [8]. Plate heat exchangers, which also are quite common, are often expensive and more difficult to maintain clean. When the equipment was sized, which can be read in section 5.0.4.3, it is described how the solution heat exchanger is considered to be two units.

Generator

After the weak LiBr-solution exited the solution heat exchanger, it enter the generator. The function of the generator is to evaporate water from the weak LiBr-solution so that the cycle can start over again. The concentrated LiBr-solution is returned to the absorber, and the water vapor enters the condenser.

In reality the generator is a shell and tube heat exchanger where the LiBr-solution is sprayed onto the tubes. The water evaporates on the shell side and the overhead stream goes in the tubes. Due to this complex setup, the generator could not be simulated as the equipment it really is in Aspen Plus. It was hence simulated as a simple separator, called *Component Separator*, where the mass

flows of the outlet streams were specified. This unit can be viewed in figure 5.3 named *GENERATO*. This was done in a way that entailed the right concentration of LiBr-solution returning to the absorber, and the right amount of water vapor returning to the preheater. However, this equipment was not true to reality either as the separation fractions was forced to be the size they were.

To verify that the right amount of water vapor would evaporate at the prevailing conditions, a flash was inserted in Aspen Plus. This can be viewed in figure 5.7. With the same streams and conditions, the same amount of water was evaporated, and the heat duty was also controlled. However, the generator does in reality operate with several equilibrium stages for a solution of LiBr and water with etylene glycol [40]. A flash unit operates as only one equilibrium stage [41]. Therefore the flash does not represent the generator perfectly either. Actually, a distillation tower would be a more accurate representation as more equilibrium stages can be taken into consideration then. However, the data needed for simulating a distillation tower, such as number of trays bottoms and reflux ratio, are unknown and do not exist in reality as it is a heat exchanger and not a tower. Hence it was considered to be unnecessary to simulate a tower in this case.

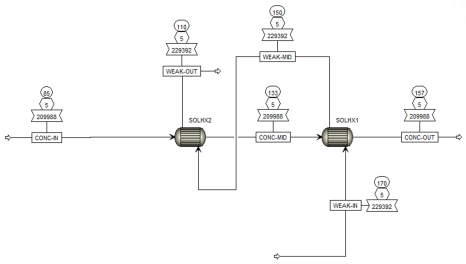

Figure 5.6: Simulation over the solution heat exchanger divided into two separate units. The temperature is showed in the circles in °C, the pressure is showed in the hexagons in bar, and the rectangles show the mass flow in kg/h.

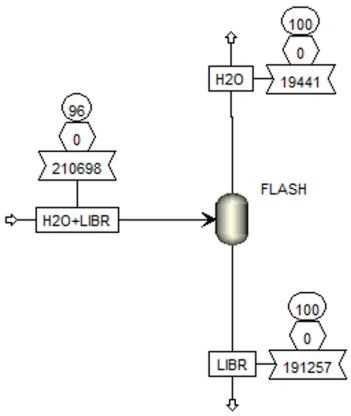

Figure 5.7: Generator simulated as a flash unit in Aspen Plus. Temperature can be seen in the circles in °C, pressure in the hexagons in bar, and mass flow in kg/h in the rectangles.

As neither the flash simulation nor the separator simulation of the evaporator were truly satisfactory approximations, one further simulation was made of a shell and tube heat exchanger. This can be seen in figure 5.8. The entire overhead flow of 360 ton/h heats the weak LiBr-solution flow so that 19.4 ton/h water evaporated, leaving the concentrated LiBr-solution. In this simulation, the ethylene glycol was disregarded as it does not evaporate in reality, where the generator operates at several equilibrium stages and ethylene glycol have a higher boiling point than water [40]. The temperature of the overhead decreases from 112 °C to 98 °C, entailing in a heat duty of 7448.75 kW at 0.1265 bar and 89 °C for the LiBr-solution.

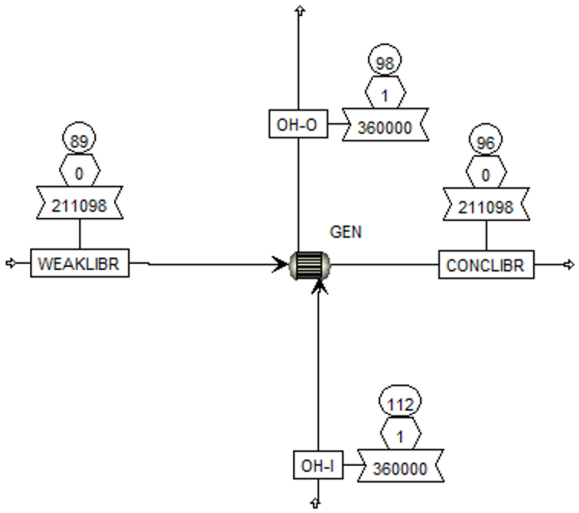

Figure 5.8: Generator simulated as a shell and tube heat exchanger in Aspen Plus. Temperature can be viewed in the circles in °C, pressure is visualized in the hexagons in bar and flows in kg/h .

Condenser

The condenser processes the water vapor exiting the generator, and condenses it with cooling water, which is sea water of 15 degrees. The cooling water was placed on the tube side, and the water vapor on the shell side. The condenser operates at the same pressure as the generator, at 0.1265 bar. Therefore it condenses at 50 °C, which can be seen in steam tables. Due to a small pressure drop affecting the temperature of condensation, the outlet temperature of the water was 48 °C. This water was later pumped back to 5 bar, before entering the preheater again, and the cycle starts over. The condenser is visualized as *COND* in figure 5.3, and in figure 5.9 in more detail.

Superheater

The stripper flow was evaporated and heated to 182 °C in the absorber. To obtain the properties of DS, with 240 °C and 9.8 bar, some additional heat was required. The heat source needed to be comparatively warm, and one such source available on the plant is HP steam. Since HP steam has a high enthalpy, only a small flow of 0.77 ton/h was needed in order to lift the stripper flow of 16.4 ton/h to 240 °C. This was simulated in a shell and tube heat exchanger in Aspen Plus, with HP steam on the tube side and the stripper flow on the shell side according to the allocation of fluids mentioned in section 4.0.2.3. The Plus simulation can be viewed in figure 5.10. As a consequence the HP steam became condensed and cooled to 199.79 °C, which is a subcooled liquid at 86 bar. Hence, this will end up in the dearators at the site, to be deoxidized and later recirculated back to the furnaces and boilers to become new steam. The DS exiting the superheater can thereafter be piped to the furnaces and used for cracking.

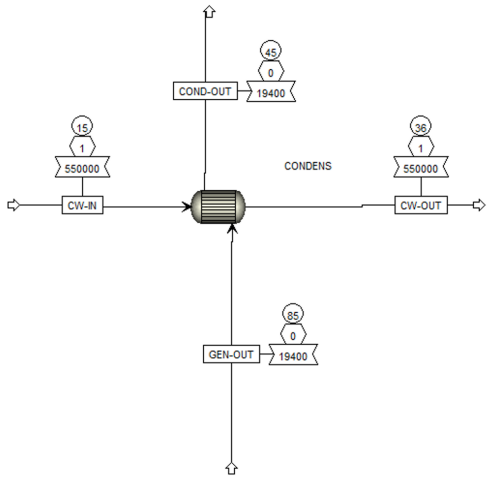

Figure 5.9: Simulation over the condenser in Aspen Plus. The temperature is showed in the circles in °C, the pressure is showed in the hexagons in bar, and the rectangles show the mass flow in kg/h.

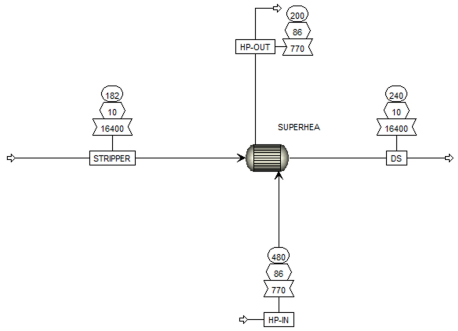

Figure 5.10: Superheater simulated in Aspen Plus. Temperature can be seen in the circles in °C, pressure in the hexagons in bar, and mass flow in kg/h in the rectangles.

Stripper Water

The path of the stripper water starts with being pressurized to 9.8 bar by a pump. This can be viewed in figure 5.12. Thereafter it is heated and evaporated in the absorber and finally superheated to the final temperature in the superheater. This was simulated in Aspen Plus where the absorber is represented by a shell and tube heat exchanger, and the superheated is represented by a heater, visualized in figure 5.11.

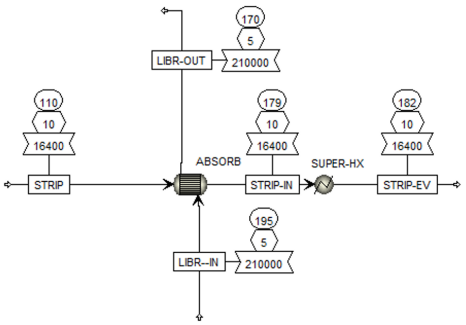

Figure 5.11: Simulation over the stripper path through the absorber and superheater. The temperature is showed in the circles in °C, the pressure is showed in the hexagons in bar, and the rectangles show the mass flow in kg/h.

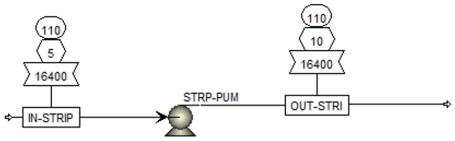

Figure 5.12: Simulation in Aspen Plus over the stripper flow being pumped to the DS pressure. The temperature is showed in the circles in °C, the pressure is showed in the hexagons in bar, and the rectangles show the mass flow in kg/h.

In all the units included in the AHT, pressure drops were entered after being computed. The pressure drops did not affect the function or conditions noticeably anywhere in the AHT.

5.0.4.3 Sizing of equipment

After the AHT was designed in Aspen Plus, it was sized both using the correlations in 4.0.2.2 in Excel to iterate a suitable design as well as designed in Aspen EDR to enable a comparison between the designs. In the preheater it was estimated that no phase changes occurred since the water was only heated, and the change of gas composition in the overhead was assumed to be negligible. The necessary values to calculate the heat exchanger design such as heat capacity, viscosity, temperatures, density conductivity, mass flows and heat exchanged were collected from the simulation in Aspen Plus. A first guess of the inner and outer diameter of the tubes, length of heat exchanger, number of tube passes, shell diameter and the overall heat transfer coefficient U was made.

From the initial guesses, the area required could be calculated by 5.1.

$$A_{tot} = \frac{Q}{\Delta T_{lm} U F_t} \tag{5.1}$$

The number of tubes was then calculated as in 5.2.

$$N_t = \frac{A}{d_o \pi l N_{tube\ passes}} \tag{5.2}$$

From this, the flow rate in the tubes could be estimated as in 5.3.

$$v_\infty = \frac{\dot{m}}{N_t \rho \pi \frac{d_i^2}{4}} \tag{5.3}$$

The flow rate on the shell side was estimated by equation 5.4.

$$v = \frac{\dot{m}}{\rho \pi (\frac{d_s hell^2}{4} - N_t \frac{d_i^2}{4})} \tag{5.4}$$

The Reynolds number for both shell and tube side could then be calculated by using 4.18, Prandtl number with 4.19, the j_h factory with 4.26 and Nusselt number with 4.20. From the correlation of Nusselt number the convective heat transfer coefficient h_i and h_o could be calculated by relation 5.5.

$$h = \frac{Nu \cdot k}{d_e} \tag{5.5}$$

Finally the overall heat transfer coefficient U could be calculated by 4.16. The guessed U was then changed until the guessed U and the calculated U was of the same value. When this value was obtained the total area could be estimated. The aim of the iterative process of the U value was to optimize it without exceeding the limitations for pressure drop and velocity. These constraints can be viewed in table 4.2 and section 4.0.4. To get the value of U to be as high as possible, the shell diameter was set as low as possible without undercutting the tube bundle diameter and exceeding the shell side pressure drop nor the fluid velocities. The tube lengths, number of tube passes and tube diameters were also changed to get the highest value of U. The area of the configuration with the highest U was then chosen and used for cost calculations. To evaluate whether the chosen design could be appropriate, the pressure drop on the shell and tube side were calculated using equations 4.53 and 4.55.

In the evaporator a phase change of the water is occurring. For this heat exchanger pool boiling was assumed, with quench oil on the tube side and water on the shell side. The same procedure as for the preheater above was used with the exception that convective heat transfer coefficient h_o

was calculated from the Nusslet correlation with γ, equations 4.28 and 4.29.

The sizing of the absorber is less straightforward since a reaction and phase change is present. In reality, as the concentrated LiBr is sprayed onto vertical tubes in the absorber, the water vapor from the evaporator is absorbed into the falling film on the tubes and becomes a liquid. On the tub side, the water from the stripper is evaporated to generate DS. Since this becomes quite complex to calculate and size two estimation were made. It is assumed that the heat transfer from the phase change of water due to absorption occurs at constant temperature from the liquid solution to the stripper water. Secondly, the absorber is sized as two separate heat exchangers, one that represents the temperature decrease of the LiBr which preheats and partially evaporates the stripper water and one that represents the heat transfer from the absorption reaction which fully evaporates and superheats the stripper water.

Since the stripper water is on the tube side in the absorber instead of the shell side as in the evaporator, flow boiling is taking place instead of pool boiling. The iterative process is the same as before but the additional dimensionless numbers Bo, Co and Fr are used.

The total mass flux, G is calculated by 5.6:

$$G = \frac{\dot{m}}{N_t \pi \frac{d_i^2}{4}} \tag{5.6}$$

Co is calculated from equation 4.31, Bo from equation 4.30, Fr from equation 4.32 ψ from equation 4.33 and h_L from equation 5.5. The heat transfer coefficient for the two phase flow, h_{tp} can then, at last be calculated by 5.7:

$$h_{tp} = \psi h_L \tag{5.7}$$

U, the overall heat transfer coefficient, is as usual calculated again from equation 4.16 and iterated until it corresponds to the guessed value with a tolerance of two decimals.

Since no phase changes occur in the solution heat exchanger. The area required is calculated the same way as for the preheater. In the generator on the other hand, water is evaporating from the weak LiBr solution. In reality, the weak solution is sprayed onto the tubes and the water evaporates from the falling film. The correlations needed to calculate this correctly were, however, difficult to obtain and varied a lot depending on the solution being subjected to evaporation. The generator was thereby approximated as a shell and tube heat exchanger with pool boiling. The area was calculated the same way as for the evaporator described above, but with the overhead on the tube side instead of quench oil.

The next heat exchanger to be sized was the condenser where water condenses on the shell side and cooling water is being heated on the tube side. The general procedure is the same as for the others. Γ was calculated from equation 4.36 and the heat transfer coefficient, h for the condensation was then given from equation 4.36. The heat transfer coefficient for the cooling water was calculated from equation 5.5 as for the preheater.

Lastly, the superheater was designed, where HP steam was superheating the evaporated stripper flow exiting the absorber. In this heat exchanger, the HP steam condensed from 480 °C to 199 °C at 86 bar, that is a sub cooled liquid. Hence, equation 4.35 and 4.36 could be used for the HP flow. The stripper flow was allocated on the shell side and the HP steam flow on the tube side.

The data obtained for the calculations and sizing of the heat exchangers from Aspen Plus can be seen in table A.3 in Appendix, section A. The data for Cp, ρ, k and μ are mean values between the inlet and outlet conditions of the streams. The index t stands for the stream on the tube side and s for the shell side.

To verify that the design of the heat exchangers, especially if the number of tube passes were plausible, the heat exchangers were also designed in Aspen EDR. Graphs showing the internal temperature differences between the shell side and the tub passes were also generated enabling verification that internal temperature crosses did not occur. The graphs can be seen in A.0.4 in appendix. If the number of tub passes were too high, leading to an internal temperature cross, the number was reduced.

5.0.4.4 Piping

To determine the cost of the piping and pressure drops, the position of the AHT first had to be decided. At the cracker there is an old furnace that is no longer in use, but has not yet been removed since the area is not needed for anything else at the moment. This area could be a suitable space for the AHT. The total area that the AHT will take up was computed via a quick back-of-an-envelope calculation. The area of each heat exchanger was estimated by multiplying the lengths with the shell diameter. For the absorber and generator, the area was computed a bit differently, as they stand vertically. Hence the area they occupy is the radius squared times π. However, it was computed as the diameter squared to account for some space between the units. The area for the pumps was not computed. All the areas were summed to 55 m^2, and to account for some spacing between the units and for the pump areas, these 55 m^2 would need to be expanded a bit. The highest vertically standing heat exchanger has a height of 18 meters, so the AHT will need to be at least 18 meters high. All the AHT equipment should preferably stand close to each other to minimize piping. As there are just shell and tube heat exchangers and pumps, there would be no need to have the equipment indoors. The safety risks associated with the AHT are sufficiently low to allow it to be outdoors.

The pipes for each fluid were assumed to follow the already existing pipe routes at the plant. The minimal number of pipe bends was estimated to be nine, and then 50 % additional bends were added to accommodate for unexpected turns. The number of bends was thereby estimated to be 15 for the overhead and quench oil to the AHT, and 15 each on the way back. The distance for the overhead to the AHT, colored brown in the figure 5.13 below, was determined to be 350 m, the distance for the quench oil (the black route) was somewhat shorter, since it is a bit closer to the pipe route and was thereby estimated to 325 m. The distance was determined by measuring the distance along the route in Google Maps. From the stripper tower to the AHT, the distance was estimated to be 100 m (the blue route) with 15 bends as well. For the DS produced from the stripper water to the furnaces, the distance was assumed to be the same as for the overhead, 350 m and 15 bends. The stripper outlet is at ground level while the overhead is 30 m above ground and the quench oil is 3 m above ground.

Figure 5.13: Position and piping for the AHT. The brown line is the overhead, the black one is quench oil and the blue one is the stripper water. The red circle is the possible position of the AHT.

The pressure drops for the piping were determined by first guessing the diameter of the pipes. The velocity could then be determined by the data from table A.3 and equation 5.3. The Reynolds number was then calculated by equation 4.18 and the flow losses and head losses from equations 4.57 and 4.58. The total pressure loss was then obtained from equation 4.56 and the diameter of the pipes were then changed until a suitable pressure drop was given.

5.0.5 Cost calculations

To evaluate the AHT economically, mainly three methods were used. The PBP, ANP and the NPV, seen in 4.41, 4.43 and 4.42. In order to obtain a value of the cash flow and total investment, calculations were performed for each equipment, and for each part of the current operations that the implementation of the AHT would affect. To start of, the investment cost was computed with equation 4.39 in Excel. For shell and tube heat exchangers, the value of a is 32 000, b is 70, n is 1.2, and the variable S is the heat transfer area of the heat exchanger, computed as in 5.1. For the heat exchangers that contained LiBr-solution, stainless steel 316 was chosen as material, as LiBr is a corrosive fluid. Stainless steel was used in the absorber, solution heat exchangers and generator. The rest of the equipment: the preheater, evaporator, condenser, and superheater was considered to be made out of carbon steel since that is less expensive but assumed resilient enough. As equation 4.39 only applies for equipment made out of carbon steel, a material factor of 1.3 was added to the equipment made out of stainless steel 316 to compensate for the more expensive material. For the pumps in the AHT cycle, equation 4.39 looked a bit different. The variable a was set to 8000, b was set to 240, and n to 0.9. The variable S is in this case the pump effect in L/s. The same material factor of 1.3 was added to the LiBr-solution pump, while the water pump and stripper pump was left unchanged. Also, an isentropic efficiency η_{is}=0.85 and an electrical efficiency η_{el}=0.98 were divided from the total pump cost, two values assumed based on common efficiencies in chemical process.

The equipment cost for all heat exchangers was also computed in Aspen EDR. This was done to enable comparing the cost computed via equation 4.39 in Excel with another value. After comput-

ing the equipment cost, other investment factors such as engineering cost, piping cost, potential buildings etc needed to be taken into consideration. This was done by multiplying a Lang factor by the equipment cost. In this work, the factor 4.74 was chosen since the cracker at Borealis is considered a fluid processing plant. Also a contingency factor of 20% was added to the investment cost to allow for unexpected costs.

Since quite long pipes were considered to be needed, the costs for the pipes were computed separately in addition to the Lang factor. This was done with equation 4.40, assumed that the pipes was made out of carbon steel. The total investment cost then became the equipment cost multiplied with the Lang and contingency factors, plus the piping cost.

The cash flow included money saved from the freshwater reduction, reduced carbon dioxide emissions and reduced fuel gas usage. The additional energy consumption for implementing the AHT will be very small since it is mainly driven by waste heat. The only negative cash flows considered were electricity needed for pumps, electricity lost in the EGT as steam is taken from the HP header, plus the cost of the HP steam. By using equations 4.44 to 4.52, the cash flow can be computed.

Finally, the PBP, ANP and NPV could be computed as in equations 4.41, 4.43 and 4.42. The NPV and ANP was computed for 20 years after the investment.

Aspen EDR considers capital cost, construction and engineering man hours, while the computations in Excel with equation 4.39 only considers the equipment cost. The Lang factor considers some more parameters than only engineering cost, capital cost and construction cost, namely offsite costs and installation costs. With the Lang factor multiplied, the costs calculated by Excel hence considers some more parameters than the costs obtained from EDR. Hence the Lang factor is added to the EDR investment cost as well. Also, the heat exchanger area is normally multiplied by 110% to oversize the exchanger to account for changes in temperatures and flows. However, this was not taken into consideration in this work, since the investment cost in EDR does not consider this. In order to enable comparing the costs obtained from Excel with the costs from EDR, they need to be based on the same parameters.

5.0.6 Sensitivity analysis

In order to evaluate the effect of changes in different key parameters in the system, a sensitivity analysis was performed. Two aspects were considered, where the first aspect of the analysis covered how different operational conditions affected the performance of the AHT. The other evaluated how changes in different cost parameters affected the profitability of the AHT.

The temperature and heat of the overhead is vital for the AHT to work properly. The overhead has 112 °C at normal operating conditions. However, it sometimes decreases down to 107 ° C and some heat losses in the piping from the source of the overhead to the position of the AHT is also expected. To examine the effect of a temperature decrease, the inlet temperature of the overhead to the generator was decreased to the lowest possible temperature while still maintaining the same vapor flow of water. The overhead inlet stream to the generator can be viewed in figure 5.8.

Another analysis performed was whether temperature changes of the cooling water, which in this case is sea water, would affect the operation of the condenser. It was considered that the highest sea water temperature would be reached during summertime, at a value of 20 °C. The cooling water inlet temperature was therefore changed to 20 °C from 15 °C in order to evaluate whether the cooling effect would be worsened.

When evaluating the cost and profitability of the AHT, the current values of EU carbon permits, electricity, and natural gas and fresh water was considered. These values can however vary and will affect the PBP greatly. The current prices of CO_2 emissions per ton is 940 SEK [27]. This cost

was varied between 400 SEK/ton to 1500 SEK/ton. Further, the electricity price varies as well. Especially throughout a year in Sweden as the outdoor temperature varies greatly [42]. Electricity prices also differs depending on where in Sweden you are, and the area where Borealis cracker is located is called SE3. The cheapest prices is during summer, and 2024 the lowest price in SE3 occurred in August of 0.0854 SEK/kWh. The highest electricity price in SE3 occurred in January of 0.830 SEK/kWh. As the electricity prices could possibly increase even more in the future, the electricity price was varied between 0.09 and 1 SEK/kWh.

Moreover, the natural gas price was varied between 0.3 SEK/kWh to 1 SEK/kWh [43]. The current price of natural gas is 0.6 SEK/kWh [44].

These costs were then consequently varied to calculate maximum and minimum profitability. The cost of drinking water in the Gothenburg region is 11.64 SEK/m^3. However, Borealis cracker does not pay the same price as households, as they have their own water purification system, and take in fresh water straight from Hällungen. Therefore, these drinking water prices are assumed to be reduced with 30%, hence 11.64· 0.7=8.15 SEK/m^3. The cost of water was changed between 5-20 SEK/m^3 [45].

5.0.7 Fuel Gas

The integration of an AHT could potentially generate enough steam so that one boiler would be made redundant. The cost of producing HP steam was estimated based on the freshwater need, fuel gas consumption and boiler efficiency. The enriched methane fuel gas contains 80 mole-% methane and 20 mole-% hydrogen. Methane has an effective heating value of 50 MJ/kg and hydrogen 120 MJ/kg [46].

6
Results

In the Result section that follows, the outcome of the simulations and calculations performed will be presented. This refers to the sizing of the AHT, cost calculations, and also a sensitivity analysis of the AHT.

Regarding the simulations of the CCC and MVR, they were considered to be very unprofitable due to the large electricity demands and HP consumption. In tables A.1 and A.2 the electricity consumptions for different configurations of the CCC and MVR can be viewed. All CCCs have electricity demands between 10.7 and 21.3 MW which is considered to be unrealistic as the task was to utilize waste heat. The MVRs electricity demand was between 1.14 and 9.5 MW with additional HP steam or water injection.

Considering the AHP, it was unable to lift the temperature of the stripper flow to above 160 °C at 5 bar which is not enough for DS. Additional compression would therefore be needed to achieve 9.8 bar. This would require a lot of electricity since compression of an gas is very energy demanding and was not considered as a suitable solution.

6.0.1 Heat exchanger sizing

The final design of the heat exchangers are presented below in table 6.1, 6.2 and 6.3. A comparison of the sizing parameters for the heat exchangers designed in EDR and Excel was made. Mostly the parameters are the same in EDR and Excel. In the cases where they differ, it is because the most profitable design in Excel does not conform with the design simulated in EDR.

Table 6.1: Data from Aspen Plus for Preheater, Evaporator, and Absorber 1.

	Unit	**Pre.** Excel	**Pre.** EDR	**Evap.** Excel	**Evap.** EDR	**Abs. 1** Excel	**Abs. 1** EDR
d_o	[mm]	21	21	50	50	16	21
d_i	[mm]	16	-	46	-	12	-
l_{tube}	[m]	3.25	3.25	10	10	6	6
$n_{passes,t}$	-	6	6	2	2	1	1
d_{shell}	[m]	1.63	1.63	1.00	1.00	0.90	0.90
v_{tube}	$[\frac{m}{s}]$	0.07	-	3.50	-	0.019	-
v_{shell}	$[\frac{m}{s}]$	22.34	-	0.029	-	0.41	-
Re_{tube}	-	2 413	-	312 516	-	606	-
Re_{shell}	-	10 540	-	4 290	-	14 702	-
U	$[\frac{W}{m^2°C}]$	93.9	-	783.53	-	296.96	-
N_{tube}	-	382	167	104	83	1 576	935
A	$[m^2]$	491.65	204.7	327.66	257.1	475	364.1
ΔP_{tube}	[bar]	0.0009	0.044	0.50	0.88	0.000016	0.033
ΔP_{shell}	[bar]	0.22	0.21	0.00027	0.63	0.011	0.32
Cost	[MSEK]	1.53	1.12	1.07	0.82	1.93	1.41

Table 6.2: Data from Aspen Plus for Absorber 2 and Solution Heat Exchangers 1 & 2.

	Unit	**Abs. 2** Excel	**Abs. 2** EDR	**Sol. 1** Excel	**Sol. 1** EDR	**Sol. 2** Excel	**Sol. 2** EDR
d_o	[mm]	21	-	16	25	21	25
d_i	[mm]	16	-	12	-	16	-
l_{tube}	[m]	6	-	12	5	15	6
$n_{passes,t}$	-	2	-	1	6	1	1
d_{shell}	[m]	1.00	-	0.64	0.8	0.62	0.85
v_{tube}	$[\frac{m}{s}]$	0.022	-	0.36	-	0.28	-
v_{shell}	$[\frac{m}{s}]$	19.31	-	0.39		0.69	-
Re_{tube}	-	65	-	1 751		6 179	-
Re_{shell}	-	817 035	-	16 118	-	28 908	-
U	$[\frac{W}{m^2°C}]$	1 065	-	474.47	-	439.55	-
N_{tube}	-	744	-	997.57	163	683	571
A	$[m^2]$	588.48	-	601.41	264.8	675.87	234.9
ΔP_{tube}	[bar]	0.000037	-	0.050	0.046	0.026	0.043
ΔP_{shell}	[bar]	0.47	-	0.37	0.63	0.79	0.48
Cost	[MSEK]	2.37	-	2.42	1.11	2.72	1.07

Table 6.3: Data from Aspen Plus for Generator, Condenser, and Subcooler.

	Unit	**Gen.** Excel	**Gen.** EDR	**Cond.** Excel	**Cond.** EDR	**Sup.** Excel	**Sup.** EDR
d_o	[mm]	50	50	50	50	25	25
d_i	[mm]	46	-	46	-	21	21
l_{tube}	[m]	18	6	6	6	4.8	4.8
$n_{passes,t}$	-	3	4	8	8	1	1
d_{shell}	[m]	3.3	5	1.67	2.50	0.5	0.37
v_{tube}	$[\frac{m}{s}]$	81.06	-	0.67	-	6.19	0.28
v_{shell}	$[\frac{m}{s}]$	8.35	-	2.20	-	5.09	21.62
Re_{tube}	-	24 869	-	32 598	-	722306	-
Re_{shell}	-	5 422	-	174 275	-	34 636	-
U	$[\frac{W}{m^2°C}]$	104.26	-	362.06	-	112.76	-
N_{tube}	-	674	1 306	137	115	1	68
A	$[m^2]$	5 720.64	4 632.2	1 033	839.8	0.08	24.3
ΔP_{tube}	[bar]	0.61	0.023	0.14	0.16	0.84	0.04
ΔP_{shell}	[bar]	0.0084	0.31	0.0041	0.0018	0.0073	0.46
Cost	[MSEK]	29.82	10.56	4.25	2.47	0.33	0.48

6.0.2 Cost Evaluation

The equipment costs for each equipment included in the AHT can be viewed in table 6.4, together with the total equipment cost. As most of the heat exchangers cost calculations were performed in both Excel and Aspen EDR, these values can be compared. The equipment that lack cost calculations from EDR have the notation "−" where the cost have not been computed.

Table 6.4: Equipment cost.

Equipment	**Cost EDR [MSEK]**	**Cost Excel [MSEK]**
Preheater	1.12	1.53
Evaporator	0.82	1.07
Absorber 1	1.41	1.93
Absorber 2	-	2.37
Solution heat Exchanger 1	1.11	2.42
Solution heat Exchanger 2	1.07	2.72
Generator	10.56	29.82
Condenser	2.47	4.25
Superheater	0.47	0.33
Water Pump	-	0.44
LiBr Pump	-	3.29
Stripper Pump	-	0.40
Total equipment cost	25.53	50.57

The total investment cost for the AHT can be viewed in table 6.5. This is the equipment cost with additions of pipe costs, the Lang factor and the contingency factor. The total investment costs can be compared between the calculated values in Excel and EDR.

Table 6.5: Total Investment cost.

	EDR	Excel
Total Equipment Cost [MSEK]	25.53	50.57
Pipe cost [MSEK]	9.26	9.26
Lang Factor	4.74	4.74
Contingency Factor	1.2	1.2
Total Investment Cost [MSEK]	**197.89**	**340.31**

Beyond the investment cost, there are also cash flows considered for the implementation of the AHT. This regards water savings, fuel gas savings, CO_2-emission savings, HP steam usage and changes in electricity usage. These computations were only performed in Excel, and can be viewed in table 6.6. Revenues are noted positive while costs are noted negative.

Table 6.6: Cash flows from the implementation of an AHT.

Source	**Mass flow** $[\frac{ton}{h}]$ / $[\frac{ton}{year}]$	**Cost** $[\frac{SEK}{ton}]$	**Cost** $[\frac{MSEK}{year}]$
Water Savings	16.4 / 136 120	8.73	1.19
Fuel Gas Savings	1 / 8 300	16 330	135.57
CO_2 Emission Reduction	2.74 / 22 772.74	941.36	21.41
HP Steam Usage	0.77 / 3 691	1082.33	-6.92
Source	**El. Consumption [kW]**	**Cost** $[\frac{SEK}{kWh}]$	**Cost** $[\frac{MSEK}{year}]$
Electricity Loss	1955.54	0.39	-6.79
Electricity Usage	35.23	0.39	-0.12
Total Cash Flow			**144.34**

The results of the final cost of the project can be observed in table 6.7. The NPV and ANP are computed until 20 years after the investment was begun, and the interest rate is assumed to be 10%. The PBP, NPV and ANP are all computed with current prices of electricity, fuel gas, CO_2-emissions and fresh water. Also, all three profitability methods are computed with the investment costs computed in both Excel and EDR. These values can hence be compared in table 6.7.

Table 6.7: PBP, NPV and ANP for the AHT.

	Excel	**EDR**
PBP [years]	6.21	3.42
NPV [MSEK]	117.36	259.79
ANP [MSEK]	13.79	30.52

6.0.3 Sensitivity Analysis

A sensitivity analysis over the investment and implementation of the AHT was performed in order to evaluate whether the project would be sensitive to unpredictable possible changes in operating conditions or pricing. The parameters considered were an increase in cooling water temperature, a decrease of the temperatures in the overhead and quench oil streams, variations in electricity price and CO_2-emission cost, and changes in the fuel gas price.

6.0.3.1 Cooling Water Temperature Increase

When the cooling water temperature was increased to 20 °C in the condenser in the Aspen Plus simulation, it could be concluded that the performance of the condenser was not affected. The outlet temperature became 40.87 °C instead of 35.86 °C which it was with 15 °C at the inlet. The water vapor could still be condensed and cooled to 45 °C from 85 °C, and hence the heat duty was not affected. The increase in cooling water outlet temperature entails a smaller value of ΔT_{min} of only around 4 °C. This entails in a larger heat transfer area of 1243 m^2 instead of 1033 m^2 that was the area when the inlet temperature was 15 °C. In order to account for warmer cooling water temperatures, that occurs during summertime, the condenser would need to be designed larger. This would also entail a more expensive investment cost.

6.0.3.2 Overhead Stream Temperature Decrease

Looking at the case where the overhead heat was colder than 112 °C, the generator would be affected in such a way that the temperature difference on the overhead side became smaller. When the overhead flow consisted of only vapor, the heat transfer effect were much lower than when it was liquid, additionally the phase change itself releases a lot of energy. The lowest possible overhead inlet temperature for the generator simulated as a heat exchanger in Plus ended up to be 102 °C. In this case, ΔT on the overhead side was only 8.8 °C, instead of 14.5 °C as when the inlet temperature was 112 °C. This means that the overhead temperature could drop up to 12 °C, without negatively affecting the generator's performance.. There would be a difference in outlet temperature of the concentrated LiBr-solution and water vapor. With a overhead inlet temperature of 112 °C, the outlet temperature would be 95.84 °C, and with 102 °C it would be 95.91 °C. This is actually slightly warmer, probably because of the higher liquid content, which gives better heat transfer. As the ΔT of the overhead decreases, a larger heat transfer area would however most likely be required, which would entail a more expensive investment but not effect the operation of the AHT as a whole.

The overhead heat is also utilized in the preheater. However, the performance of the preheater will not be affected by a drop in the overhead temperature, as it uses heat from the overhead stream exiting the generator. And as it was concluded in the last paragraph, the outlet temperature of the overhead stream from the generator will not change much, and hence the preheater will not be affected by a overhead temperature decrease above 102 °C.

6.0.3.3 Quench Oil Stream Temperature Decrease

It was further tested how the evaporator would be affected if the quench oil dropped in temperature. The result from this test showed that it could drop 20 °C, from 187 °C to 167 °C without affecting the operation or performance of the evaporator. With 167 °C quench oil, the ΔT_{min} would still be 14 °C. In reality, it would be very unexpected if the temperature were to drop 20 °C, but this means that most disturbances in quench oil temperature will be harmless to the operation.

6.0.3.4 Electricity Price Variations

Different electricity prices were tested in order to evaluate the effect on the PBP. The result can be viewed in table 6.8. Depending on the season, the electricity prices vary. Therefore the mean value of 0.41 SEK/kWh for electricity price over a year will be used as an approximate cost. It can also be seen that the PBP varies a lot between the values computed from Excel or EDR.

Table 6.8: Varied electricity prices affect on the PBP computed in Excel and with EDR.

Electricity Cost $[\frac{SEK}{kWh}]$	PBP (Excel) [years]	PBP (EDR) [years]
0.09	5.62	3.09
0.41	6.21	3.42
1.00	7.72	4.25

6.0.3.5 Fuel Gas Price Variations

Looking at table 6.9, the PBP for different fuel gas prices can be seen. Some make up in the form of natural gas is used to complement the fuel gas in the furnaces. The implementation of the AHT will reduce the need for this and the effect of the natural gas price variation on the PBP is evaluated accordingly.

Table 6.9: Varied natural gas cost affect on the PBP computed in Excel and with EDR.

Natural gas cost [$\frac{SEK}{kWh}$]	PBP (Excel) [years]	PBP (EDR) [years]
0.30	10.93	6.02
0.60	6.21	3.42
1.00	3.94	2.17

6.0.3.6 CO_2-emission Price Variations

In table 6.10 the PBP for variations in CO_2-emission pricing can be viewed. The CO_2-amount considered is the reduction of CO_2-emissions from implementing the AHT.

Table 6.10: CO_2-emission price affect on the PBP computed in Excel and with EDR.

CO_2-emission price [$\frac{SEK}{ton}$]	PBP (Excel) [years]	PBP (EDR) [years]
400	7.26	4.00
940	6.21	3.42
1500	5.41	2.98

6.0.3.7 Freashwater Price Variations

In table 6.11, variations in PBP for different prices of fresh water can be viewed. It should be noted that the fresh water savings by implementing the AHT are considered, hence the fresh water price affects the income.

Table 6.11: Fresh water price variations and how they affect the PBP.

Fresh water price[$\frac{SEK}{m^3}$]	PBP (Excel) [years]	PBP (EDR) [years]
5	6.27	3.45
8.15	6.21	3.42
20	6.02	3.32

6.0.3.8 Extreme Case Scenarios

In table 6.12, the value of the highest versus the lowest PBP possible can be studied. For the lowest PBP, the fuel gas price, CO_2-emission price and water price is on the upper edge while the electricity price is at the lower edge. On the contrary, for the highest PBP, the fuel gas price, CO_2-emission price and water price are low, and the electricity cost is high. However, it is not realistic that these prices stay the same over the entire PBP.

Table 6.12: Fuel gas prices, electricity prices, CO_2-emission prices and water prices configured so that the highest and lowest PBP possible is achieved.

Price_{fuel} $[\frac{SEK}{kWh}]$	Price_{el} $[\frac{SEK}{kWh}]$	Price_{CO_2} $[\frac{SEK}{ton}]$	Price_{water} $[\frac{SEK}{m^3}]$	PBP (Excel) [y]	PBP (EDR) [y]
1.00	0.09	1500	20	3.34	1.84
0.3	1.00	400	5	28.10	15.47

However, in reality, the fuel gas price is correlated to the electricity price, and considering this the two extreme cases seen in table 6.13 below was produced.

Table 6.13: Fuel gas prices in correaltion with electricity prices, together with CO_2-emission prices and water prices configured so that the highest and lowest PBP possible is achieved.

Price_{fuel} $[\frac{SEK}{kWh}]$	Price_{el} $[\frac{SEK}{kWh}]$	Price_{CO_2} $[\frac{SEK}{ton}]$	Price_{water} $[\frac{SEK}{m^3}]$	PBP (Excel) [y]	PBP (EDR) [y]
0.30	0.09	1500	20	4.00	7.27
1.00	1.00	1500	20	**2.19**	3.98
0.30	0.09	400	5	6.56	**11.91**
1.00	1.00	400	5	2.79	5.06

6.0.3.9 Evaluation of Differences in Cost Between EDR and Excel

It cannot be overlooked that the Excel costs are much higher than the EDR costs throughout all cost calculations. To be able to determine what was the cause of this difference, the areas computed via EDR were inserted into the cost equation 4.39 in Excel. The comparison between the investment costs for areas computed via EDR and Excel with equation 4.39 can be seen in table 6.14, plus the cost computed in EDR completely.

Table 6.14: Investment cost computed via equation 4.39 for heat exchanger areas computed via EDR and Excel.

Investment cost computed with Excel area with eq.4.39 [SEK]	220.10
Investment cost computed with EDR area with eq.4.39 [SEK]	166.43
Investment cost computed completely in EDR	90.37

6.0.3.10 Steam System Impact

The impact of the steam system created by the AHT regards the HP steam of 0.77 ton/h used to superheat the stripper flow, plus the fact that one boiler, that produces at least 15 ton/h of HP, is considered to be taken out of operation as DS steam is produced from the AHT instead.

7
Ethics

Fresh water is a scarce resource on Earth. Only 2.5% of Earth's water is freshwater, of which only 0.3% is contained in rivers, lakes, and the atmosphere, the rest is contained in glaciers and groundwater [47]. For a long time, there has been an excess of fresh water in Sweden [48]. The use of water has therefore been somewhat careless and little effort has been made to reuse water and reduce the fresh water consumption. The industries in Stenungsund constitute 70% of the fresh water consumption in Stenungsund. Water in the municipality of Stenungsund is now becoming so scarce that it limits the production of new buildings in the region. To enable enough drinking water for the inhabitants, a new water pipe with water from the neighboring municipality, Kungälv, was put into operation in 2024.

Borealis is the single largest consumer of fresh water in the municipality and is at its limit of maximum allowed water outtake from Lake Hällungen. Borealis' steam cracker consumes 1.3 Mm^3 per year and the municipality of Stenungsund uses 1.9 Mm^3 per year. The industries' consumption of fresh water therefore greatly affects the inhabitants of Stenungsund. Reduction of the water consumption at the industries could enable better access of drinking water. There are, however, little incentive for industries to make such investments since the low cost of water in Sweden makes it difficult to justify them. Incentives to make the investments are instead the uncertainty if water access will be reduced in the future. Since industries in Sweden are accustomed to a certain purity and ease of access to water, the requirements of water purification for different processes are often neither known nor investigated and water from different streams are often combined. In this study the purity of the stripper water was assumed to be adequate both based on information from Borealis and a previous study stating 50 ppm of phenols was acceptable in a steam cracking furnace [36]. Since no further purification is assumed to be needed, both the complexity and cost of the project is reduced and the incentive to invest in it is increased.

It is expected that climate change will increase the number of days with low water flow. During the summers, this figure will change from 20 to 50-80 days in the region [48]. The population in Stenungsund is also expected to increase by 15 % from 2021 until 2030. Borealis' cracker is also using more than their assigned water rights and are dependent on Vattenfall to provide them with water of 0.3 Mm^3/year. Vattenfall can terminate the contract with one-year notices. It can therefore be necessary for Borealis to reduce their water consumption even though the revenue from it is not sufficiently high.

Another benefit from the installation of an AHT to reduce the water consumption with excess heat is the reduction in need of fuel gas and consequently the reduction in CO_2 emissions. During 2024, the emissions of Borealis' cracker amounted to 618 kton CO_2 [49]. A reduction of fuel gas burning in the boilers to produce steam could potentially reduce the emissions with 18 kton per year, a reduction of 3%. As CO_2 is a GHG which leads to global warming and climate change [50], it is of great importance to reduce the CO_2 emissions. Climate change leads to fluctuations in seasons, low rainfall, and temperature rise which in its turn leads to lower output of agriculture globally. Health problems as a consequences of droughts and floods will increase as well as diseases due to extreme weather conditions.

8

Discussion

In the following section, a discussion will be conducted in order to evaluate the design, operation, cost and environmental effects of an integration of the AHT.

8.0.1 Choice of Heat Pump Design

The AHT was considered to be the only appropriate solution based on the task at hand. CCCs and MVRs are more established types of heat pumps but are not suitable for this application. The CCC has a very high electricity demand which would make it unlikely to be profitable. The MVR had a lower electricity demand but instead used HP steam to evaporate the stripper flow. Almost as much HP steam was needed as the amount of DS generated. This also means that no waste heat was utilized and there would have been no reduction in fuel gas use, only the freshwater demand. Since an AHP uses both a high temperature and a low temperature heat source to generate a medium temperature output, the heat generated was not high enough to evaporate the stripper water at 9.8 bar, only at 5 bar. To generate DS it would therefore also need to be compressed. This would consume a lot of electricity, as stated previously. Due to all this, the AHT was deemed to be the best solution.

8.0.2 Differences in Cost Estimate Methods

It can be seen that for all heat exchangers where the equipment costs have been calculated in Excel or EDR in table 6.4, the numbers are of the same order of magnitude. However, the reason why the numbers are not more similar could depend on the choice of correlations used for the calculations in Excel. For example in the evaporator, generator, superheater and condenser, the streams undergo a phase change, which means that more complex correlations were used when computing the heat transfer numbers, such as equation 4.35 or 4.28. As these depend on more variables than the simplest correlations for the heat transfer number, there are more factors that could affect the end result. Some values, such as the heat transfer friction factor and the F_t-correlation factor are taken from a diagram for the Excel calculations. These values hence need to be iterated manually, and could contribute to a more unsure result. The variables used in the heat transfer number calculations are taken from Aspen Plus, and the EDR costs are also based on the Plus model. However, in Excel a mean value for the different values have been used, generating a linearity of the values. In EDR on the other hand, each value is being calculated. As can be seen in the temperature-length diagrams (in figures A.2 to A.8 in Appendix, section A.0.4) the temperature profiles for the heat exchangers are not always linear, effecting the properties such as heat capacity, viscosity etc. The calculations in Excel does not take non-linear temperature profiles into consideration.

Other parameters that could differ between EDR and calculations in Excel are assumptions in the heat exchanger design. Aspects such as number of baffles, baffle spacing, tube pitch and tube arrangement have been selected based on common settings found in literature [8]. However, these design parameters are assumptions, and may not be the same choices that Aspen Plus or Aspen EDR calculates with. Also, these design parameters may not be the best suited for the application.

For example, looking at the tube arrangement, the calculations for the shell side heat transfer factor j_h in Excel assumes the tube arrangement that gives the highest heat transfer number. The tube arrangement is then chosen in the j_h-diagram so that the factor j_h becomes as large as possible. In Aspen EDR another tube arrangement may have been chosen. Hence, the tube arrangement may differ between the EDR and Excel designs, which could lead to differences in cost. The same goes for baffle spacing. In the Excel calculations the baffle spacing and tube pitch are computed via equations 4.54 and 4.24, while they are chosen by EDR when designed there. Thus, there are several assumed design parameters for the shell and tube heat exchangers that may differ between the calculation in Excel and EDR, that could affect the cost. Other parameters that could possibly contribute to this difference is the material cost, as the cost of carbon steel and stainless steel 316 could vary depending on country and time. The price of the material that EDR used was unknown.

Especially the generator differs a lot in cost comparing the EDR design with the Excel computations. As described in section 4.0.1.4, the generator is in fact a shell and tube heat exchanger where the LiBr-solution is sprayed onto vertically oriented tubes wherein the overhead flow goes, and water is boiling on the shell side. This configuration is considered to be quite difficult to simulate. Hence it is simulated as a flash column, a simple separator and a shell and tube heat exchanger in Aspen Plus. None of these simulations gives a design that is true to reality. The same goes for EDR, where it is designed as a normal shell and tube heat exchanger. These approximations, in both Excel and EDR, would give rise to uncertainties in the cost.

Despite these large difference in investment cost of the generator, no more simulations was made. The explanation to this is that there was a lack of time, and if there was more time available, the generator could have been simulated in other programs that allow complex heat exchanger configurations such as spray on vertical tubes with falling film theory. This also applies for the absorber, which was also difficult to simulate correctly.

8.0.3 Sensitivity

It can further be discussed that the AHT is fairly robust as it can handle relatively high temperature drops in both the overhead stream and quench oil, as well as an increase in cooling water temperature. Since the cycle includes two pumps and a valve, the AHT is easily regulated with regards to pressure.

8.0.4 Effect on Steam System

If the AHT were to be implemented, the same amount of DS to the furnaces would still be needed. At the moment DS is produced from HP steam that has either been reduced by an electricity generating turbine, a compression turbine or by a reduction valve. By generating DS directly from the stripper water the amount of HP steam in the steam system would be reduced. As the three boilers often operate at minimum load, a reduction in the amount of HP steam would have to be made by shutting down one of the boilers. If more HP steam would be required due to the operating conditions, the load of the remaining two boilers can be increased. Dividing the load on two boilers instead of three could also be beneficial since the efficiency usually is higher when equipment is not operating at minimum load.

8.0.5 Requirements of Water Purity

Water for production of HP steam needs to be very pure because high pressure and temperature generating very corrosive conditions. DS steam is of both lower pressure and temperature, and

should therefore not require as pure water. The water from the stripper contains at most 50 ppm phenols. For ethylene steam cracking furnaces, 50 ppm is an acceptable level [36] of oil content in the DS. However, fouling problems can occur in the absorber and superheater, as 16.4 ton DS contains 0.82 kg phenols. A possible solution to avoid excessive fouling from phenols could be to use a thermosiphon. The thermosiphon uses a pressure difference between the inlet and outlet to drive the flow through the reboiler [51]. A regular shell and tube heat exchanger heats the liquid containing water with phenols to a mixture of gas and liquid. The flow is thereafter separated to gas and liquid, where the liquid is recirculated back to the heat exchanger. Over top goes the vapor that is purified from phenols. Part of the liquid flow can be bled out through the bottom and sent to the BET to avoid accumulation of phenols. This structure can be seen in figure A.9 in Appendix A. It can further be discussed that a thermosiphon would not add significantly to the total cost, as it is similar to a shell and tubr heat exchanger, that the absorber already is. However since a part of stripper water will be bled out, a larger flow will likely be used and the heat exchanger will be a little larger. Another solution beside the thermosiphon could be to use the water from the BET since this water is purified from phenols. Using this water at about 30 °C would entail a DS flow of 14.3 ton/h, which would decrease the efficiency of the AHT.

8.0.6 Redundance

Moreover, it can be discussed that redundant equipment could be needed for the operation of the AHT to work smoothly. For instance, the three pumps should have redundancy for oil changes and possible operation errors. For maintenance such as removal of fouling in the heat exchangers, the two remaining boilers can be operated at higher load to enable taking the AHT out of operation for regular cleaning.

8.0.7 Profitability Evaluation

To answer the question whether it is possible to design an integration that is economically favorable for the process: it depends on the circumstances. Since the investment cost and PBP differs so much between the two methods of computing the cost, there is no obvious conclusion that can be drawn regarding profitability. Moreover, looking at the extreme cases in table 6.12, a PBP of 28.10 years is compared with one of 1.84 years. This is a very large range, and a more realistic approach would be to assume that the electricity price correlates with the fuel gas price. For this case, the PBP varies between 2.19 and 11.91 years instead. As the water prices and CO_2-emission prices probably will not decrease in the future, it would be more realistic to assume a PBP closer to the lower value of 2.19 years. It was concluded earlier that a project with a PBP over 3.5 years usually is considered to be unworthy to invest in.

The cost estimated in this thesis is very approximate and if the AHT were to be integrated in reality the cost is assumed too be within +/- 50 % of the final cost. For the cost calculated from Excel this would change the PBP from 6.21 to 9.32 years or 3.12. For the EDR cost it would change from 3.42 to 5.13 or 1.71 years.

8.0.8 Possible Future Aspects

Today, the fuel gas is either sold or used by the furnaces and boilers, but this could potentially change in the future as more and more renewable sources of energy are being used in society. One solution to this problem could be to separate the fuel gas into methane and hydrogen, where the methane could be sold on the natural gas network. Another solution could be to use the methane for the synthesis of methanol [52].

The Borealis cracker cannot avoid generating fuel gas as it is a by-product from the cracking process. For it to be sold, it requires that there is a fuel gas or natural gas demand. It could be that this demand decreases in the future as society moves towards using more renewable fuels. If the fuel gas cannot be sold, it needs to be used by the furnaces, boilers or sent to the flare. Hence the revenue of the AHT implementation would decrease due to increased CO_2-emission costs, and the investment would be less profitable. A possible solution to this could be to separate the fuel gas into pure methane and hydrogen which could enable synthesizing it to methanol.

The integration of the AHT is not only a question of economy, but also environment. Even though the investment itself might not that profitable, an implementation of the AHT, or another solution to reduce the freshwater intake, might be necessary since the fresh water intake is at its upper limit. CO_2-emission reduction will also be beneficial since the prices likely will increase. Hence a balance between cost and environment needs to be regarded.

Another possible solution for utilizing the overhead waste heat with the AHT could be to generate district heating instead. District heat is of a much lower temperature than DS, which means that an AHP could be used instead of an AHT. Since an AHP has a much higher COP than an AHT the heat output would be higher. However, this application would not solve the problem with reducing fresh water intake.

9
Conclusion

This thesis aimed to investigate how the freshwater intake at Borealis cracker plant in Stenungsund could be reduced by regenerations of steam. The first question to be answered was how much steam could be recovered. This work lead to the conclusion that 16.4 ton/h DS could be generated through the implementation of an AHT. This also means that 16.4 ton/h fresh water can be saved. It could further be concluded that the steam system at the cracker plant would not be affected by the implementation of the AHT in any significant way. Only 0.77 ton/h HP steam is used in the superheater, and a potentially smaller HP steam generation resulting from removing a boiler is not a must, as this generation depends on the operation conditions of the two remaining boilers.

Moreover, it was concluded that 8300 ton/year of fuel gas and 18 200 ton/year CO_2-emissions could be saved by implementing the AHT to the Borealis cracker plant.

Another question answered in this work is that the water exiting the stripper does not need to be purified any further, and can be generated into DS directly.

Lastly, it would be brave to state whether the integration of the AHT would be economically favorable or not. Due to the large fluctuations in cost depending on prices of electricity, fresh water, fuel gas and CO_2-emissions, it can be concluded that the AHT investment is sensitive. As can be seen in section 6.0.3, the PBP varies heavily between the two extreme case scenarios, and it can hence not be stated whether the investment would be profitable or not. To evaluate this further, a more detailed investigation of future price predictions would be required.

A

Appendix 1

A.0.1 CCC

In figure A.1, temperature and pressure intervals for some common working fluids can be found [8].

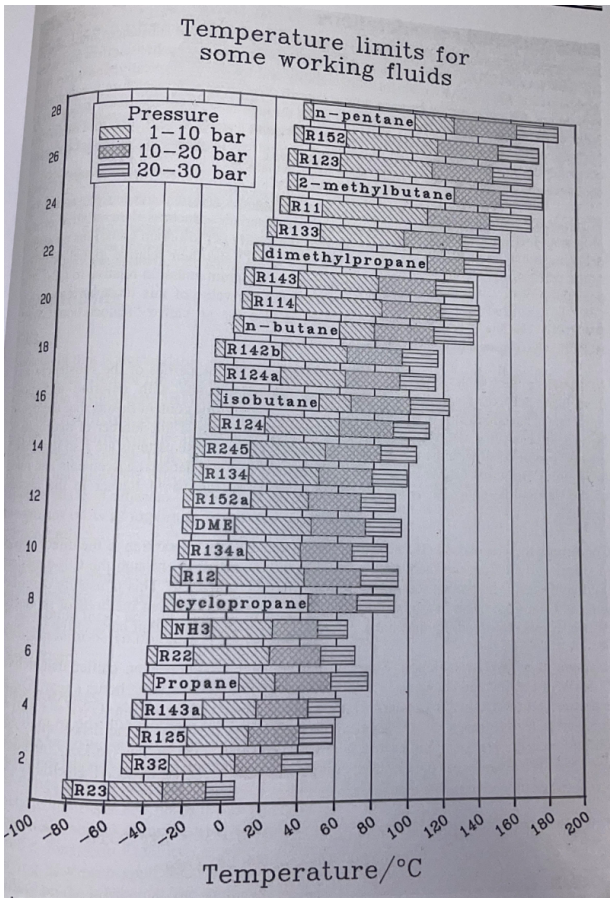

Figure A.1: Temperature limits for some working fluids.

In table A.1, properties and performances of different refrigerants simulated in a CCC in Aspen Hysys can be viewed.

Table A.1: Properties and performance of different refrigerants simulated.

Refrig.	**Boiling Point [°C]**	**Temp. lift [K]**	**El. Demand [MW]**	**Heat Output [MW]**	$\frac{HeatOutput}{El.Demand}$
R-113	48	51.9	12	55	4.58
R-141b	32	74.5	14	60	4.29
R-134a	-26	94.1	17	53	3.12
R-11	23	69	21.3	58.2	2.73
Water	100	295	10.7	-	-

A.0.2 MVR

Table A.2 show properties and performances of different MVR and compressor configurations simulated in Aspen Hysys.

Table A.2: Properties and performance of different MVR configurations simulated.

Case	**DS gen.** $[\frac{ton}{h}]$	**El. Demand [MW]**	**HP/water Demand** $[\frac{ton}{h}]$
Water injection after compression (58 °C) *	15.84	1.2	0.97 water
Water injection after compression (35°C)**	17.88	1.61	9.8 water
HP pump and HP injection prior to compression	130	9.5	100 HP
Two compressors in series with water injection	7.09	1.24	1.05 water
Intermediate cooling and two compressors (58°C)*	6.04	1.14	-
Intermediate cooling and two compressors (35°C)**	8.08	1.52	-
HP heat exchanger before compressor	50	2.46	41 HP

* The MVR heat pump uses heat from 112°C to 58°C in the overhead, in other words the first eight heat exchangers.
** The MVR heat pump uses all the heat in the overhead, from 112°C to 35°C.

It could be seen that the MVR heat pump with water injection after compression generates almost 18 tonnes per hour of DS steam, while only demanding 1.61 MW of electricity. This configuration takes all heat available in the overhead, from 112 to 35°C. In comparison to the same configuration where only the first eight heat exchangers are taken into account, using all heat entails in a 34% higher electricity demand, and generates 13% more DS steam. The electricity demanded for this increase of steam generation might be considered to be unfavorable. Hence the

MVR using heat from 112 to 58°C with water injection after compression seems to be the most favorable alternative.

A.0.3 AHT

Table A.3: Data from Aspen Plus for heat exchanger calculations.

	Pre.	**Evap.**	**Abs. 1**	**Abs. 2**	**Sol.**	**Gen.**	**Cond.**	**Sup.**
Cp_t $[\frac{J}{kg \cdot K}]$	4188.12	1952.47	4032.75	2921.95	2146.16	1991.37	4180.22	3408.5
Cp_s $[\frac{J}{kg \cdot K}]$	2016.28	3084.33	2460.18	2409.48	2359.7	1955.94	2089.90	2022.88
ρ_t $[\frac{kg}{m^3}]$	978.88	643.26	485.62	12.22	1455	1.10	996.5	448.41
ρ_s $[\frac{kg}{m^3}]$	1.17	495.17	1333.00	1376.33	1365.44	1.67	495.13	4.56
k_t $[\frac{W}{m^3 \cdot K}]$	0.65	0.12	0.68	0.28	0.25	0.041	0.61	0.37
k_s $[\frac{W}{m^3 \cdot K}]$	0.051	0.35	0.29	0.27	0.29	0.25	0.33	0.04
μ_t $[Pa \cdot s]$	0.00047	0.00033	0.00018	0.00007	0.00354	0.00017	0.00094	0.000081
μ_s $[Pa \cdot s]$	0.000052	0.00017	0.00045	0.0052	0.00052	0.0013	0.00031	0.000017
$\dot{m}_t$ $[\frac{kg}{s}]$	5.39	389.69	4.56	4.56	58.33	100	5.39	0.21
$\dot{m}_s$ $[\frac{kg}{s}]$	33.33	5.39	63.72	63.72	63.72	63.83	152.78	4.56
$T_{in,t}$ [°C]	45	187	110	179	132.70	112	15	480
$T_{out,t}$ [°C]	84	171.03	179	181.76	156.56	94.5	36	199.79
$T_{in,s}$ [°C]	94	87.95	195	195	170	84.9	85	182
$T_{out,s}$ [°C]	85	153	170	195	150	85.1	45	240
Q [kW]	969	12 975	3 662	7 086	2 967	9 914	13 319.8	524.29
ρ_{liq} $[\frac{kg}{m^3}]$	-	962.09	888.13	888.13	-	962.09	990.20	48.31
ρ_{vap} $[\frac{kg}{m^3}]$	-	2.54	5.04	5.04	-	0.28	0.07	1.51
σ $[\frac{N}{m}]$	-	0.0611	0.0611	0.043	-	0.080	0.069	0.038
a_L $[\frac{m^2}{s}]$	-	0.00000016	-	-	-	0.000000085	-	-
Δh $[\frac{kJ}{kg}]$	-	2103.22	2 018 450	2 018 450	-	2 148	2 392	2490

A.0.4 Temperature-Length Diagrams for All Heat Exchangers in the AHT.

In figures A.2 and A.3, the temperature-length diagrams for the preheater and evaporator can be viewed.

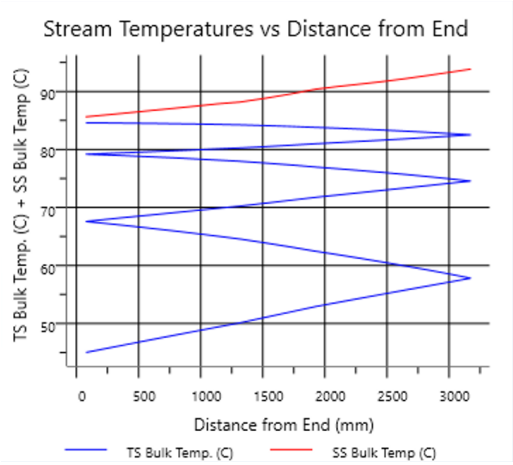

Figure A.2: Temperature-length diagram of the preheater simulated in Aspen EDR.

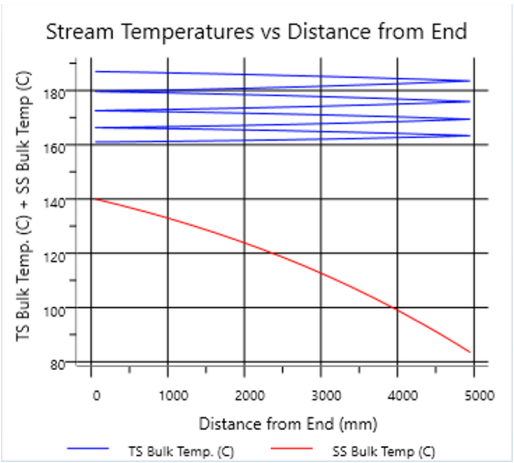

Figure A.3: Temperature-length diagram of the evaporator simulated in Aspen EDR.

Figures A.4 and A.5 show the temperature-length diagrams for the generator and condenser.

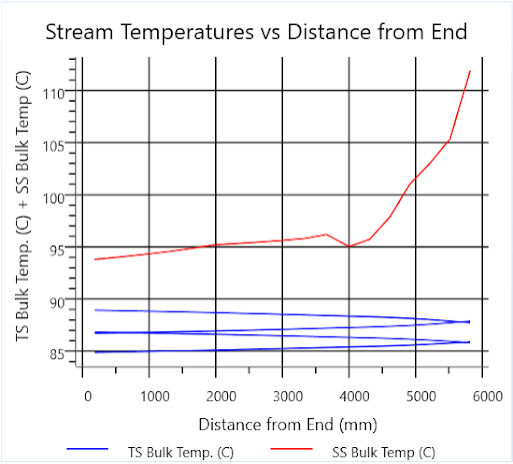

Figure A.4: Temperature-length diagram of the generator simulated in Aspen EDR.

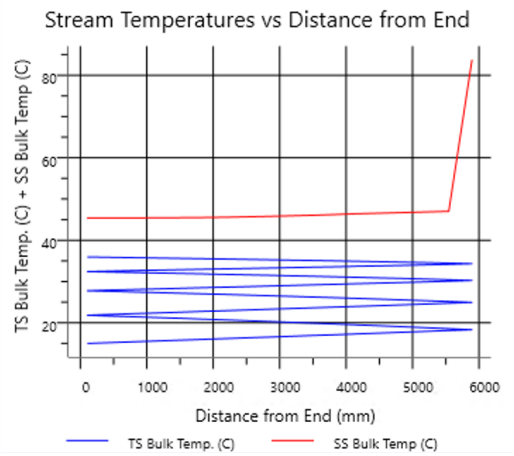

Figure A.5: Temperature-length diagram of the condenser simulated in Aspen EDR.

In figures A.6 and A.7, the temperature-length diagrams for the solution heat exchangers can be seen.

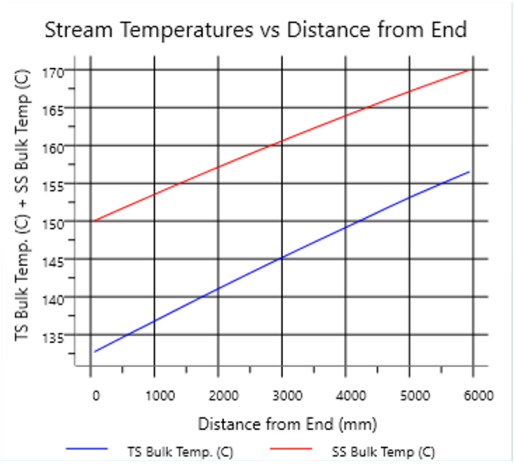

Figure A.6: Temperature-length diagram of the first solution heat exchanger simulated in Aspen EDR.

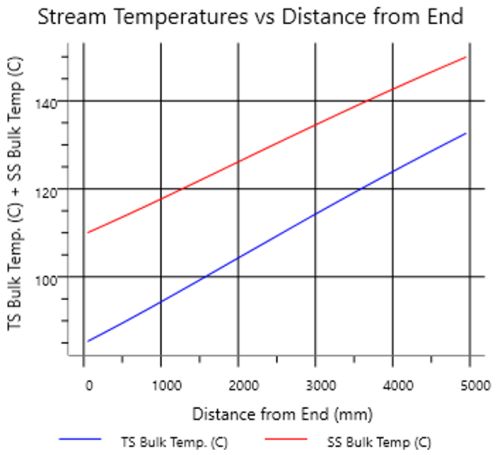

Figure A.7: Temperature-length diagram of the second solution heat exchanger simulated in Aspen EDR.

Figure A.8 Visualize the temperature-length diagram for the superheater.

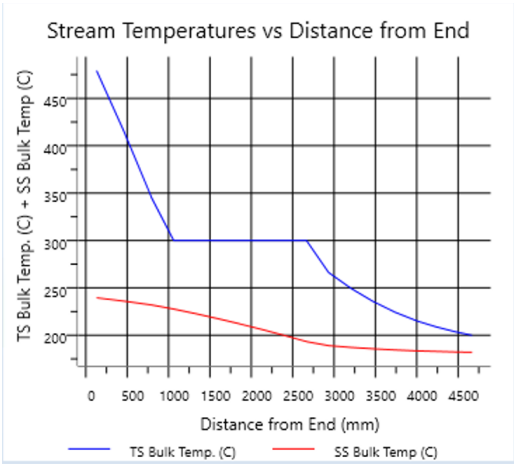

Figure A.8: Temperature-lenght diagram of the superheater simulated in Aspen EDR.

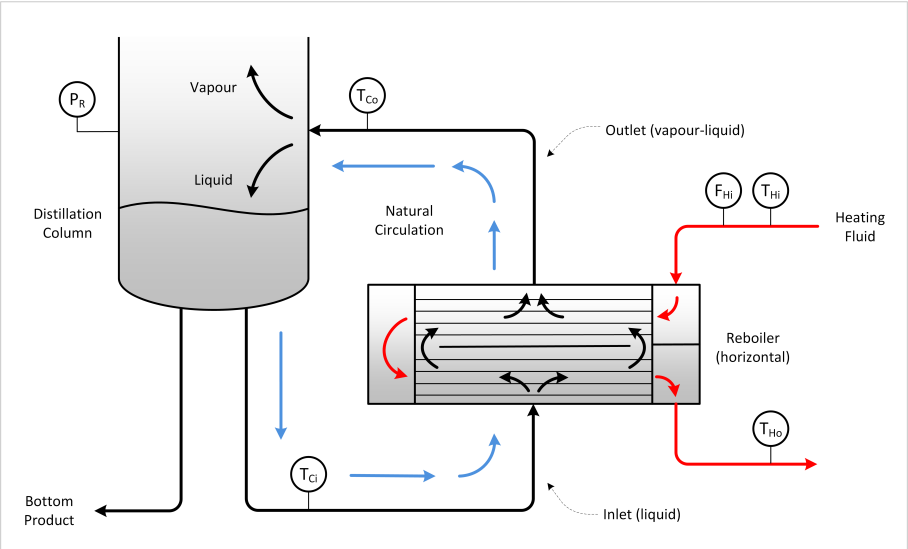

Figure A.9: Schematic representation of a horizontal thermosiphon [51].

Bibliography

[1] *Abuot borealis*. [Online]. Available: https://www.borealisgroup.com/about-us.

[2] E. E. Agency. "Water scarcity conditions in europe". (2025), [Online]. Available: https://www.eea.europa.eu/en/analysis/indicators/use-of-freshwater-resources-in-europe-1.

[3] RISE. "Industry needs to reduce its water consumption". (), [Online]. Available: https://www.ri.se/en/industry-needs-to-reduce-its-water-consumption.

[4] H. Thunman, S. Andersson, P.-E. Bengtsson, B. Leckner, and D. Pallerés, "Combustion engineering", pp. 3.2–3.23, 2020.

[5] K. Chua, S. Chou, and W. Yang, "Advances in heat pump systems: A review", *Applied Energy*, vol. 87, no. 12, pp. 3611–3624, 2010, ISSN: 0306-2619. DOI: https://doi.org/10.1016/j.apenergy.2010.06.014. [Online]. Available: https://www.sciencedirect.com/science/article/pii/S030626191000228X.

[6] H. Bauer, J. Ehrmaier, L. Gigliotti, F. Liebach, T. Schleyer, and A. Simoncini, "Industrial heat pumps: Five considerations for future growth", *Industrials Electronics Practice, McKinsey Company*, 2024.

[7] V. Wilk and G. Drexler-Schmid, "1st heat pump technology circle", *AIT Austrian Institute of Technology GmbH*, 2025.

[8] M. Ryden, L. Smultron, V. Stenberg, and M. Vigoureux, *Design of Industrial Energy Equipment*. 2021, pp. 7-1–7-12, 4-1–4-92, 6-1–6-14, 8-1–8-14.

[9] J. R. Elliott and C. T. Lira, *Introductory Chemical Engineering Thermodynamics*, 2nd ed. Prentice Hal, 2017, pp. 76–77, ISBN: 978-0-13-606854-9.

[10] X. Zhenyuan and R. Wang, "Absorption heat pump for waste heat reuse: Current states and future development", *Frontiers in Energy*, 2017. DOI: https://doi.org/10.1007/s11708-017-0507-1.

[11] *Safety Data Sheet Lithium bromide*. CHEMOS, 2021. [Online]. Available: https://www.chemos.de/import/data/msds/GB_en/7550-35-8-A0023443-GB-en.pdf.

[12] *Safety Data Sheet Ammonium, anhydrous*. CHEMOS, 2021. [Online]. Available: https://www.chemos.de/import/data/msds/GB_en/7664-41-7-A0052472-GB-en.pdf.

[13] K. Parham, M. Khamooshi, D. B. K. Tematio, M. Yari, and U. Atikol, "Absorption heat transformers – a comprehensive review", *Renewable and Sustainable Energy Reviews*, vol. 34, pp. 430–452, 2014. DOI: https://doi.org/10.1016/j.rser.2014.03.036. [Online]. Available: https://www.sciencedirect.com/science/article/pii/S136403211400197X.

[14] F. Cudok, N. Giannetti, J. L. C. Ciganda, *et al.*, "Absorption heat transformer - state-of-the-art of industrial applications", *Renewable and Sustainable Energy Reviews*, vol. 141, 2021, ISSN: 1364-0321. DOI: https://doi.org/10.1016/j.rser.2021.110757. [Online]. Available: https://www.sciencedirect.com/science/article/pii/S1364032121000526.

[15] S. Zhang, J. Luo, R. Zheng, X. Wang, G. Chen, and Q. Wang, "Vapor pressure of aqueous hcook solution as working fluids of an absorption heat transformer at high temperature", *Journal of Chemical Engineering Data*, vol. 65, 2020. DOI: https://pubs.acs.org/doi/10.1021/acs.jced.9b00745.

[16] E. Samiento-Bustos, J. G. Rodriguez, J. Uruchurtu, G. Dominguez-Patiño, and V. Salinas-Bravo, "Effect of inorganic inhibitors on the corrosion behavior of 1018 carbon steel in the libr+ethylene glycol+h2o mixture", *Corrosion Science*, vol. 50, no. 8, pp. 2296–2303, 2008, ISSN: 0010-938X. DOI: https://doi.org/10.1016/j.corsci.2008.05.014. [Online]. Available: https://www.sciencedirect.com/science/article/pii/S0010938X08001704.

[17] *Corrosion and inhibition process of carbon steel in libr-h2o solution*, 2019. DOI: 10.1007/s12206-019-0549-x. [Online]. Available: https://doi.org/10.1007/s12206-019-0549-x.

[18] H. Li, N. Russell, V. Sharifi, and J. Swithenbank, "Techno-economic feasibility of absorption heat pumps using wastewater as the heating source for desalination", *Desalination*, vol. 281, pp. 118–127, 2011. DOI: https://doi.org/10.1016/j.desal.2011.07.049. [Online]. Available: https://www.sciencedirect.com/science/article/pii/S0011916411006631.

[19] *Design of Industrial Energy Equipment*. 2021, pp. 4-1–4-50.

[20] J. R. Welty, G. L. Rorrer, and D. G. Foster, *Fundamentals of Momentum, Heat and Mass Transfer*. John Wiley Sons Singapore, 2015, vol. 6, pp. 204–205, 197–198, 147–148, 181–195, 71–73, ISBN: 978-1-118-80887-0.

[21] H. E. W. Publisher, *Shell tube heat exchangers: Thermal design and optimization*, 2023. [Online]. Available: https://heat-exchanger-world.com/shell-tube-heat-exchangers-thermal-design-and-optimization/.

[22] S. Suk, S.-Y. Lee, and Y. S. Jeong, "A survey on the impediments to low carbon technology investment of the petrochemical industry in korea", *Journal of Cleaner Production*, vol. 133, pp. 576–588, 2016, ISSN: 0959-6526. DOI: https://doi.org/10.1016/j.jclepro.2016.05.132. [Online]. Available: https://www.sciencedirect.com/science/article/pii/S0959652616306047.

[23] G. Towler and R. Sinnott, *CHEMICAL ENGINEERING DESIGN: PRINCIPLES, PRACTICE AND ECONOMICS OF PLANT AND PROCESS DESIGN*. Elsevier, 2022, ISBN: 978-0-12-821179-3.

[24] *How to calculate the weight of carbon steel tube?* [Online]. Available: https://www.hu-steel.com/news364_1013.html.

[25] *Seamless price pipe list*, 2023. [Online]. Available: https://www.vijaysalescorp.com/msl-price-list.

[26] European Commission. "About the eu emissions trading system (eu ets)". (2024), [Online]. Available: https://climate.ec.europa.eu/eu-action/eu-emissions-trading-system-eu-ets/about-eu-ets_en.

[27] T. Economics, *Eu carbon permits*, 2025. [Online]. Available: https://tradingeconomics.com/commodity/carbon.

[28] T. F. Scientific, *Safety data sheet*. [Online]. Available: https://www.fishersci.com/store/msds?partNumber=L117500&productDescription=LITHIUM+BRMID+PWD+PURIF+500G&vendorId=VN00033897&countryCode=US&language=en.

[29] CDH, *Lithium molybdate*. [Online]. Available: https://www.cdhfinechemical.com/images/product/msds/38_5948644_LITHIUMMOLYBDATE-CASNO.13568-40-6-MSDS.pdf.

[30] Sigma$_A$*ldrich*, *Safety data sheet*, 202r. [Online]. Available: https://www.sigmaaldrich.com/SE/en/sds/sial/324558?srsltid=AfmBOooQReg7oxNbEV-IFY7miElStgUOF7sZxZqCo1TOceDwHB-5nBjx.

[31] Fisher, *Safety data sheet*, 2015. [Online]. Available: https://www.fishersci.com/content/dam/fishersci/en_US/documents/programs/education/regulatory-documents/sds/chemicals/chemicals-p/S25462.pdf.

[32] K. W. Brown and T. J. Armstrong., *Hydrocarbon inhalation*, 2023. [Online]. Available: https://www.ncbi.nlm.nih.gov/books/NBK470289/.

[33] Y. Lizhong, F. Weicheng, Z. Xiaodong, and W. Qing'an, *Analysis of fire and explosion hazards of some hydrocarbon–air mixtures*. Elsevier, 2001, vol. 84, pp. 123–131. DOI: https://doi.org/10.1016/S0304-3894(01)00216-3. [Online]. Available: https://www.sciencedirect.com/science/article/pii/S0304389401002163.

[34] *Introduction to pressure equipment*. [Online]. Available: https://www.hse.gov.uk/pressure-systems/about.htm.

[35] J. Darlaston and J. Wintle, *Safety factors in the design and use of pressure equipment*. Elseveier, 2007, vol. 14, pp. 471–480. DOI: https://doi.org/10.1016/j.engfailanal.2005.08.004. [Online]. Available: https://www.sciencedirect.com/science/article/pii/S1350630706000975#bbib2.

[36] Q. Liu, H. Li, H. Zhu, S. Feng, Q. Yang, and H. Lu, "Novel purification of oily process water from ethylene production at pilot scale", *Journal of Water Process Engineering*, vol. 52, p. 103 548, 2023, ISSN: 2214-7144. DOI: https://doi.org/10.1016/j.jwpe.2023.103548. [Online]. Available: https://www.sciencedirect.com/science/article/pii/S221471442300065X.

[37] C. F. Beaton, "Steam tables", in *Heat Exchanger Design Handbook*, 1986. DOI: https://dx.doi.org/10.1615/AtoZ.s.steam_tables. [Online]. Available: https://www.thermopedia.com/content/1150/.

[38] Z. Lan, X. Ma, Z. Hao, and R. Jiang, "Experiments on saturated vapor pressure of aqueous lithium bromide solution at high temperatures", *International Journal of Refrigeration*, vol. 76, pp. 73–83, 2017, ISSN: 0140-7007. DOI: https://doi.org/10.1016/j.ijrefrig.2016.11.025. [Online]. Available: https://www.sciencedirect.com/science/article/pii/S0140700717300518.

[39] M. Ronald and S. Paul, "Modelling implementation and simulation of a single-effect absorption chiller in merit", 2010. [Online]. Available: https://www.researchgate.net/publication/267364154_Modelling_Implementation_and_Simulation_of_a_Single-Effect_Absorption_Chiller_in_MERIT.

[40] F. Schaal, K. Schilling, and H. Hasse, "Separation efficiency of thin-film evaporators: Experiments with water–ethylene glycol and methanol–water and stage-based modeling", *Chemical Engineering and Processing: Process Intensification*, vol. 47, no. 2, pp. 209–214, 2008, ISSN: 0255-2701. DOI: https://doi.org/10.1016/j.cep.2007.02.018. [Online]. Available: https://www.sciencedirect.com/science/article/pii/S0255270107001110.

[41] M. Iggland and M. Mazzotti, "Introduction to chemical engineering for lecture 7: Flash distillation", ETH Zurich, Institute of Process Engineering, Sonneggstrasse 3, CH-8092 Zurich, Switzerland, Tech. Rep., 2015. [Online]. Available: https://ethz.ch/content/dam/ethz/special-interest/mavt/process-engineering/separation-processes-laboratory-dam/documents/education/tvt%20exercises/notes_2020/ICE_Script_Flash.pdf.

[42] Elbruk, *Elpriser 2024*. [Online]. Available: https://www.elbruk.se/elpris-historik-2024.

[43] K. Energimarknadsbyrå, *Elpriser - prognos och utveckling*, 2025. [Online]. Available: https://www.energimarknadsbyran.se/el/dina-avtal-och-kostnader/elpriser-statistik/elpriser-prognos-och-utveckling/.

[44] K. Energimarknadsbyrå, *Billigast just nu för konsumenter i västsveriges gasnät*, 2025. [Online]. Available: https://www.energimarknadsbyran.se/gas/dina-avtal-och-kostnader/gaspriskollen/billigast-gaspris-just-nu/.

[45] *Vatten- och avloppstaxa*, 2025. [Online]. Available: https://goteborg.se/wps/portal/start/bygga-bo-och-leva-hallbart/vatten-och-avlopp/avgifter-for-vatten-och-avlopp/vatten--och-avloppstaxa.

[46] W. N. Assosiation, *Heat values of various fuels*, 2020. [Online]. Available: https://world-nuclear.org/information-library/facts-and-figures/heat-values-of-various-fuels.

[47] K. N. Kikkas and S. V. Kulik, "Modelling the effect of human activity on fresh water extraction from the earth's reserves", *IOP Conference Series: Earth and Environmental Science*, vol. 180, 2018. DOI: 10.1088/1755-1315/180/1/012017. [Online]. Available: https://iopscience.iop.org/article/10.1088/1755-1315/180/1/012017/meta#references.

[48] L. L, S. A, and G. P, "Vattenanvändning och möjligheter till vattenbesparing hos kemiklustret i stenungsund", RISE, Tech. Rep., 2022. [Online]. Available: https://urn.kb.se/resolve?urn=urn:nbn:se:ri:diva-62523.

[49] Borealis, *Borealis ab stenungsuns miljörapport 2024*, 2024. [Online]. Available: https://www.borealisgroup.com/sverige/h%C3%A5llbarhet.

[50] K. O. Yoro and M. O. Daramola, "Chapter 1 - co2 emission sources, greenhouse gases, and the global warming effect", in *Advances in Carbon Capture*, M. R. Rahimpour, M. Farsi, and M. A. Makarem, Eds., Woodhead Publishing, 2020, pp. 3–28, ISBN: 978-0-12-819657-1. DOI: https://doi.org/10.1016/B978-0-12-819657-1.00001-3. [Online]. Available: https://www.sciencedirect.com/science/article/pii/B9780128196571000013.

[51] A. W. Sloley, "Properly design thermosyphon reboilers", *Chemical Enginering Progress*, 1997. [Online]. Available: https://www.scribd.com/document/255677804/Sloley-Properly-Design-Thermosyphon-Reboilers.

[52] A. Caballero and P. J. Pérez, *Methane as raw material in synthetic chemistry: the final frontier*. Royal Society of Chemistry, 2013. DOI: https://doi.org/10.1016/S0304-3894(01)00216-3. [Online]. Available: https://www.sciencedirect.com/science/article/pii/S0304389401002163.

DEPARTMENT OF CHEMISTRY AND CHEMICAL ENGINERRING
CHALMERS UNIVERSITY OF TECHNOLOGY
Gothenburg, Sweden
www.chalmers.se

CHALMERS
UNIVERSITY OF TECHNOLOGY